ELSEVIER

Contents lists available at ScienceDirect

# Journal of Anthropological Archaeology

journal homepage: www.elsevier.com/locate/jaa



# Check for updates

# Regional household variation and inequality across the Maya landscape

Whittaker Schroder <sup>a,\*</sup>, Timothy Murtha <sup>b</sup>, Charles Golden <sup>c</sup>, Madeline Brown <sup>d</sup>, Robert Griffin <sup>e</sup>, Kelsey E. Herndon <sup>e</sup>, Shanti Morell-Hart <sup>f</sup>, Andrew K. Scherer <sup>f</sup>

- <sup>a</sup> Department of Anthropology, The University of Florida, Gainesville, FL 32611, USA
- <sup>b</sup> Department of Anthropology, The University of North Carolina at Charlotte, Charlotte, NC 28223, USA
- <sup>c</sup> Department of Anthropology, Brandeis University, Waltham, MA 02453, USA
- <sup>d</sup> Department of Anthropology, University of Maryland, College Park, MD 20742, USA
- <sup>e</sup> Earth System Science Center, University of Alabama in Huntsville, Huntsville, AL 35899, USA
- f Department of Anthropology, Brown University, Providence, RI 02912, USA

#### ARTICLE INFO

Keywords:
Maya
Lidar
Inequality
Gini
Household archaeology
Landscape Archaeology

#### ABSTRACT

The emergence and expansion of inequality have been topics of household archaeology for decades. Traditionally, this question has been informed by ethnographic, ethnohistoric and/or comparative studies. Within sites and regions, comparative physical, spatial, and architectural studies of households offer an important baseline of information about status, wealth, and well-being, especially in the Maya lowlands where households are accessible in the archaeological record. Between sites, more research is necessary to assess how these physical measurements of household remains compare. This paper investigates the intersection of landscape, household, and community based on a multi-scalar analysis of households using the Gini index across southeastern Mexico, in the context of a broader study of land use, land management, and settlement patterns. Notably, this paper represents a region-wide analysis of nearly continuous LiDAR data within and outside of previously documented prehispanic Maya settlements. While we conclude that the Gini index is useful for establishing a comparative understanding of settlement, we also recognize that the index is a starting point to identify other ways to study how household to community-level social and economic variability intersects with diverse ecological patterns. Highlighting the opportunities and limitations with applying measures like the Gini index across culturally, temporally, and geographically heterogeneous areas, we illustrate how systematic studies of settlement can be coupled to broader studies of landscape archaeology to interpret changing patterns of land management and settlement across the Maya lowlands.

# 1. Introduction

The origins and dynamics of economic inequality are fundamental themes of the archaeology of complex societies (Beck and Quinn, 2022; Flannery and Marcus, 2012; Kohler and Smith, 2018; Kurnick, 2015; McGuire, 2022; Paynter, 1989; Smith et al., 2018). As academic and popular voices condemning the inequitable distributions of wealth and power in modern nations have grown louder in recent decades (Graeber, 2011; Piketty, 2020, 2014; Stiglitz, 2015; Wilkerson, 2020), some archaeologists have declared the emergence, growth, and persistence of inequality as one of the discipline's grand challenges (Kintigh et al., 2014). Contemporary assessments of inequality employ various measures of material wealth including: individual and household income, accumulated wealth, consumption and expenditures, and quality of life

among others (Basri and Lawrence, 2020, 690; Coulter, 1989; Trapeznikova, 2019). In addition to material wealth, other forms of embodied, symbolic, relational, and social wealth (Bourdieu, 1986; Smith et al., 2010; Wilkerson, 2020) are important metrics for assessing inequality, yet remain challenging to document archaeologically (Smith et al., 2010). Nonetheless, because inequality impinges on every aspect of social life, it leaves material signatures that are archaeologically accessible (Kintigh et al., 2014, 9).

Borrowing from modern economic analyses, some archaeologists have adopted the Gini index – a quantitative comparison of the differential distribution of wealth within a population – as one means of measuring the material signatures of inequality through several different proxies (Amiel and Cowell, 1999; Brown et al., 2012; Chakravarty, 1990; Dorfman, 1979; Gastwirth, 1972; Giorgi, 1990; Ready

E-mail address: wschroder@ufl.edu (W. Schroder).

<sup>\*</sup> Corresponding author.

and Power, 2018; Sen, 1973; Xu, 2003). In archaeology, the use of the Gini index to assess prestige differentiation has typically focused on site-level approaches (Hutson and Welch, 2021), with additional studies at the neighborhood, district, or polity level (Thompson et al., 2021b) because these scales offer the sample populations on which archaeologists typically focus. The increasing accessibility of LiDAR and remotely sensed big data, however, offers the potential to adopt regional and landscape perspectives (Chase et al., 2012; Chi et al., 2016; Evans, 2016; VanValkenburgh and Dufton, 2020), thereby enabling macro-regional scale populations to be used as the unit of analysis.

In this paper, we use publicly available LiDAR data collected by NASA Goddard's LiDAR, Hyperspectral, and Thermal Imager (G-LiHT) over southeastern Mexico and annotated by the authors to compare Gini coefficients across diverse ecological and cultural contexts. These data provide a series of cross sections covering portions of southeastern Mexico and the Maya area. Despite the limited width (300 m) of the transects, the spatial extent of the total length of the survey encompasses diverse socioecological contexts. Prior engagement with Gini coefficients in Mesoamerica has generally centered on site-based approaches (Chase, 2017; Hutson and Welch, 2021; Smith et al., 2014), with promising ongoing research into multiscalar analyses at the regional, polity, and district levels (Thompson et al., 2021b). The present study adopts a landscape-level approach by investigating house size variability across a large region. Because the G-LiHT data were sampled without input from archaeologists, these transects provide a "pseudorandom" or "off-site" perspective (covering understudied areas distant from the largest known archaeological sites), presenting a unique opportunity to interpret regional differentiation in house size across the Maya Lowlands, especially outside of the largest urban centers. Given the novelty and scope of these data and this analytical approach, we therefore highlight general trends in the data, rather than focusing on the absolute values of the Gini indices, although we compare our findings to prior site-based and regional research into Maya inequality.

The benefit of the G-LiHT data is their spatial coverage; however, a limitation is that the transects reflect a palimpsest of Maya settlement with great time depth. While we cannot yet incorporate temporal data into this analysis, we take the first step to interpret household-level wealth differentiation based on house size across the Northern, Central, and Western Maya Lowlands through remote sensing. We also discuss other limitations of this method with further plans to incorporate the larger built environmental and agrarian context of these data into future studies. Throughout our analysis, we urge discretion when interpreting Gini coefficients in archaeological contexts, clearly outlining and problematizing the methods used, while we remain optimistic that largescale comparisons of statistical differentiation can have relevance to our understanding of inequality in past societies.

We first offer an overview of the Gini index and related studies of inequality in archaeology. Next, we discuss the G-LiHT dataset and methods of analysis, before presenting our results. We conclude that while absolute values of Gini coefficients vary based on different architectural metrics, including structure and patio group footprint area and volume, these values correlate positively with each other across the dataset. Furthermore, we observe weak correlations between Gini indices and several cultural and environmental variables, including settlement density, agricultural terrace density, and rainfall. Additional patterns emerge when Gini coefficients are compared across physiographic sub-regions of the Maya lowlands.

# 2. Overview of the Gini index

Over the past decade, some archaeologists have adopted the Gini index – originally applied to modern, capitalist industrial economies – to model the relative inequality of wealth distribution in pre-modern societies (Bogaard et al., 2019; Kohler et al., 2017; Smith et al., 2014). The Gini index is one of many measurements of statistical dispersion and is commonly applied by economists to household income data to assess

inequality (Chakravarty, 1990; Peterson and Drennan, 2018). Although wealth may be directly measured through income data, wealth inequality also manifests in human societies through differential access to material goods or resources (material or financial capital), social ties or opportunities (social capital), status or credentials (symbolic or cultural capital) or health and skills (human capital) (Bourdieu, 1986). Adding additional complexity to assessing wealth inequality, archaeologists typically lack written records of household income, and instead must rely on proxies for wealth, such as household size, agricultural landholdings, or artifact assemblages (Smith, 1987).

In the Maya context, assessing wealth inequality is often approached through a combination of architectural, artistic, epigraphic, and ethnohistoric sources. Scott Hutson (2020) notes that although researchers have historically characterized Maya society as having two classes (elites and nonelites), more recent evidence points to multiple economic and social groups within Maya society. Rather than reflecting the presence of a "middle class" (Chase and Chase, 1996; Smith, 2018), the diversity of Maya social groups might be meaningfully differentiated based on vocation, including royalty, nobles, craftspeople, merchants, farmers, and other-than-human agents (Harrison-Buck and Hendon, 2018; Houston and Inomata, 2009). Despite the lack of evidence for a formal bureaucracy among the Classic period Maya, epigraphy reveals diverse sets of titles relating to inherited noble duties in royal courts (Foias, 2013; Inomata and Houston, 2018; Jackson, 2013; Miller and Brittenham, 2013). This perspective notes the existence of both social and economic hierarchies in Maya society, but that individual and household attributes vary within groups. Hutson (2020, 411) also notes the benefits of continuous variables (e.g. house size or labor metrics) for assessing wealth and inequality. Based on these metrics, he further points to the lack of clear "strata" in Maya society, highlighting one strength of the Gini index, namely that the distribution of wealth across a community can be assessed and visualized.

As a measure of wealth dispersion, the Gini index is closely linked to the Lorenz curve, first proposed and developed by Max Lorenz (1905). The Lorenz curve is a graphical representation of wealth concentration within a population, showing the cumulative proportion of income or wealth that is owned by a cumulative proportion of the population. This curve is then compared against a line of equality extending from the origin point at a 45° angle to the point where 100% of cumulative income is shared by 100% of the cumulative population. The line of equality represents a hypothetical population where wealth or income is distributed equally. Lorenz (1905) observed that the curves of unequal distributions will always intersect with the line of equality at the lowest and uppermost ends, but the degree to which the bow formed by the Lorenz curve projects away from the line of equality represents the magnitude of inequality in the population.

Corrado Gini (1912) proposed that this degree of inequality could be quantified by calculating the ratio of the area between the line of equality and the Lorenz curve over the total area under the line of equality (the latter typically equal to 0.5), yielding a value known as the Gini coefficient, ranging from 0 to 1. A coefficient of 0 would indicate that the Lorenz curve and the line of equality are the same, expressing an equal distribution, while a coefficient of 1 would theoretically occur if the Lorenz curve protruded to its maximum extent, representing maximal inequality. Mathematically, the Gini coefficient is equivalent to half of the relative mean absolute difference of a distribution, represented by the following formula, where G is the Gini coefficient, n is the number of observed values, x is a single observation, and  $\overline{x}$  is the sample mean:

$$G = \frac{\sum_{i=1}^{n} \sum_{j=1}^{n} |x_i - x_j|}{2n^2 \overline{x}}$$

While potentially meaningful, the Gini coefficient reduces the complexity of inequality distributions to a single value. Adrian Chase (2017, 35) has noted that two distinct populations can exhibit the same Gini coefficient while producing Lorenz curves with very different

forms. Chase has further argued that the shape of a Lorenz curve can reveal inflection points, or "kinks," that may reflect clearly defined social classes with significant wealth disparities. In contrast, a curve without such inflection points will be smoother without sudden changes in slopes. However, kinks will also be more discernible in the Lorenz curves generated with small sample sizes.

Small sample sizes can additionally produce inaccurate results when calculating the Gini coefficient. Several researchers (Bowles and Carlin, 2017; Deltas, 2003) have observed that Gini coefficients calculated from small sample sizes tend to underestimate inequality; for example, even when a single individual holds all wealth within a small population, the Gini coefficient will fall short of 1. To compensate for small sample bias, the calculation of a corrected or unbiased Gini coefficient based on sample size will ensure the value varies over the unit interval (Bowles and Carlin, 2017, 2), represented by the following formula, where  $G_{\rm C}$  is the corrected, adjusted, or unbiased Gini coefficient, G is the uncorrected or biased Gini coefficient, and  $\Pi$  is the number of observed values:

$$G_C = G \frac{n}{n-1}$$

Confidence intervals are additional metrics that help to describe and compare Gini coefficients, especially important to consider when working with small sample sizes, as confidence intervals will be wider for small versus large sample sizes. These confidence intervals ensure the quantification of the extent to which hypothetical extreme values absent from the sample might affect the calculation of the Gini coefficient, which is less likely to occur in larger samples. The most common approach uses bootstrapping to select repeated random samples (generally at least 1,000) of the same size at a given confidence level (80–95%) (Dixon et al., 1987; Peterson and Drennan, 2018, 53; Thompson et al., 2021b, 10). The result will be a lower and upper confidence Gini coefficient, providing an error range at the specified confidence level.

Several archaeological publications and online tutorials outline the methods to calculate Gini coefficients, typically relying on a spreadsheet approach to tally cumulative proportions (Chase, 2017; Smith et al., 2014). This workflow can be automated in the R statistical software environment, and the DescTools (Tools for Descriptive Statistics) package (R Core Team, 2021; Signorell, 2022), among others. Within the DescTools package, the Gini function can calculate the biased and corrected Gini coefficients from a vector of values (which can be imported from a spreadsheet or data frame), as well as the confidence intervals using bootstrapping. These data can be output to a spreadsheet for visualization, or Lorenz curves can be visualized in R using the generic plot function or the ggplot2 and gglorenz packages (Chen and Cortina, 2020; Wickham, 2016).

While the methods behind the calculation of Gini coefficients and the generation of Lorenz curves are straightforward, the interpretation of these metrics is more challenging. Although developed to measure inequality, these models are fundamentally measures and visualizations of statistical dispersion. When applied to known metrics of income or wealth distribution, this statistical dispersion unquestionably relates to economic inequality. However, when applied to any other metric, the onus is on the researcher to establish the correlation between inequality and their chosen metric. Christian Peterson and Robert Drennan (2018, 41), for example, prefer to use the term "differentiation" to highlight the diversity of a given metric across a population, possibly although not necessarily correlated with inequality.

When applied to archaeological data, the Gini coefficient is unlikely to reflect directly income or wealth. Archaeologists, therefore, must select measurable proxies that they can justify as reasonable indicators of household wealth in past societies (Chase, 2017; Peterson and Drennan, 2018; Smith, 1987; Thompson et al., 2021b). The first archaeological application of the Gini coefficient evaluated the use of Lorenz curves with examples of metrics of inequality including material goods and agricultural landholding (McGuire and Netting, 1982;

McGuire, 1983, 104-105). Other methods have incorporated data related to grave sizes, forms, and goods (Munson and Scholnick, 2022; Schulting, 1995; Windler et al., 2013; Yu, 2019). In Mesoamerica, Michael E. Smith and colleagues (2014) argued that in addition to agricultural field size, house size is an appropriate measure of household wealth. According to Smith and colleagues (2014, 312), in agrarian societies, elite houses are generally larger, more elaborate, and more costly than those of commoners. The explanation for the correlation between wealth and house size is that larger houses are more costly to construct in terms of material, time, and labor, and wealthier households often intentionally build large and elaborate homes to signal their prestige (Smith et al., 2014, 312). In addition to household size, archaeologists have investigated construction labor costs and materials as a means of assessing wealth (Abrams, 1994; Hutson, 2020; Strawinska-Zanko et al., 2018). House size can be integrated into an analysis of Gini coefficients in several ways, including structure footprint area, structure height, surface area, volume, or some combination of these metrics. Archaeological studies of inequality of house sizes generally adopt structure footprint area or structure volume (Barnard, 2021; Brown et al., 2012; Chase, 2017; Smith et al., 2014; Thompson et al., 2021b). These metrics are useful proxies for inequality in the Maya area, where researchers have identified in ethnographic contexts that house size is primarily related to wealth rather than necessarily to population size (Netting, 1982; Strawinska-Zanko et al., 2018; Wilk, 1983).

Researchers, however, are presented with an interpretive challenge to select which structures represent the "house," and how the eminently mappable remnants of such structures may be conceptually mapped to a social "household." In the Maya area, the first researchers to examine settlement patterns and household archaeology systematically adopted the Principle of Abundance. This heuristic argues that because all people need a residence, and such buildings are typically less costly than dedicated religious or political architecture (e.g., temples and palaces), most mounded features found by archaeologists across the landscape were domestic structures (Ashmore and Willey, 1981). However, the smallest of these features could not house individuals or their families and were deemed ancillary structures for storage (Lamoureux-St-Hilaire, 2022). The specific threshold separating houses from ancillary structures would have varied regionally, but a cutoff of 8 square meters has been proposed (Ashmore, 1981; Liendo Stuardo, 2002, 59). Furthermore, even as the inclusion of pyramids or ballcourts would improperly skew the data, certain large structures represented elite residences or palaces that should not be omitted from the calculation of Gini coefficients. To complicate the matter, such residences additionally included public space and living quarters for servants and other nonelite individuals. Smith and colleagues (2014, 319-320) presented a methodology for estimating living space within apartment compounds at Teotihuacan; however, this approach must be further developed to be applied to other cultural contexts.

As noted above, an additional challenge is whether single structures represent Maya households. In reality, Maya households are better mapped not onto single buildings, but instead onto entire domestic architectural compounds oriented around plazas (called patio or plazuela groups), as well as space outside of houses, including residential terraces, yards, gardens, and agricultural fields (Chase, 2017; Nelson, 2005, 137; Robin, 2003, 314; Thompson et al., 2021b). Archaeologists must also consider that Maya homes were periodically expanded over time and built over earlier phases of construction (McAnany, 2013). When these additions represent continuous occupation, architectural volume can be included as an aspect of accumulated wealth, an assumption of the Principle of First Occupancy, that the largest households represent the oldest families in a settlement (Ashmore, 1991; Blackmore, 2011a, 174, Blackmore, 2011b, 88; McAnany, 2013). However, if a structure is reoccupied after abandonment, its volume might reflect the wealth of distinct households across large scales of time. An additional complication with volume estimates is that values are calculated based on the mounded rubble left behind by collapsed

buildings, not the volume of houses or superstructures themselves, many of which were built with perishable materials. Still, in certain subregions of the Maya Lowlands, for example the Puuc hills, structure volume may provide a better proxy for differentiation due to the verticality of construction of the largest houses. Across the Maya lowlands, larger structure volumes may correlate with the presence of vaulted buildings that correlate with wealth and status (Estrada-Belli et al., 2023).

Furthermore, not all houses across the landscape were necessarily occupied at the same time and deciding which structures to include in an analysis of inequality will affect the results. In this sense, many of the challenges facing the interpretation of inequality alongside structure size are shared by the reconstruction of population estimates (Canuto

et al., 2018). Resolving these issues can be accomplished by establishing consistent and clearly defined methodologies through collaboration with other researchers, as well as comparing how the use of different metrics affect the results of Gini indices.

#### 3. Dataset

The LiDAR data used in this analysis were collected in 2013 by NASA Goddard's LiDAR, Hyperspectral, and Thermal Imager (G-LiHT) as part of a REDD + study over southeastern Mexico (Cook et al., 2013; Golden et al., 2016). While these data were collected with single flight transects measuring approximately 300 m wide, the combined length of the study over southeastern Mexico amounts to 3,200 km and a total area of 1,118

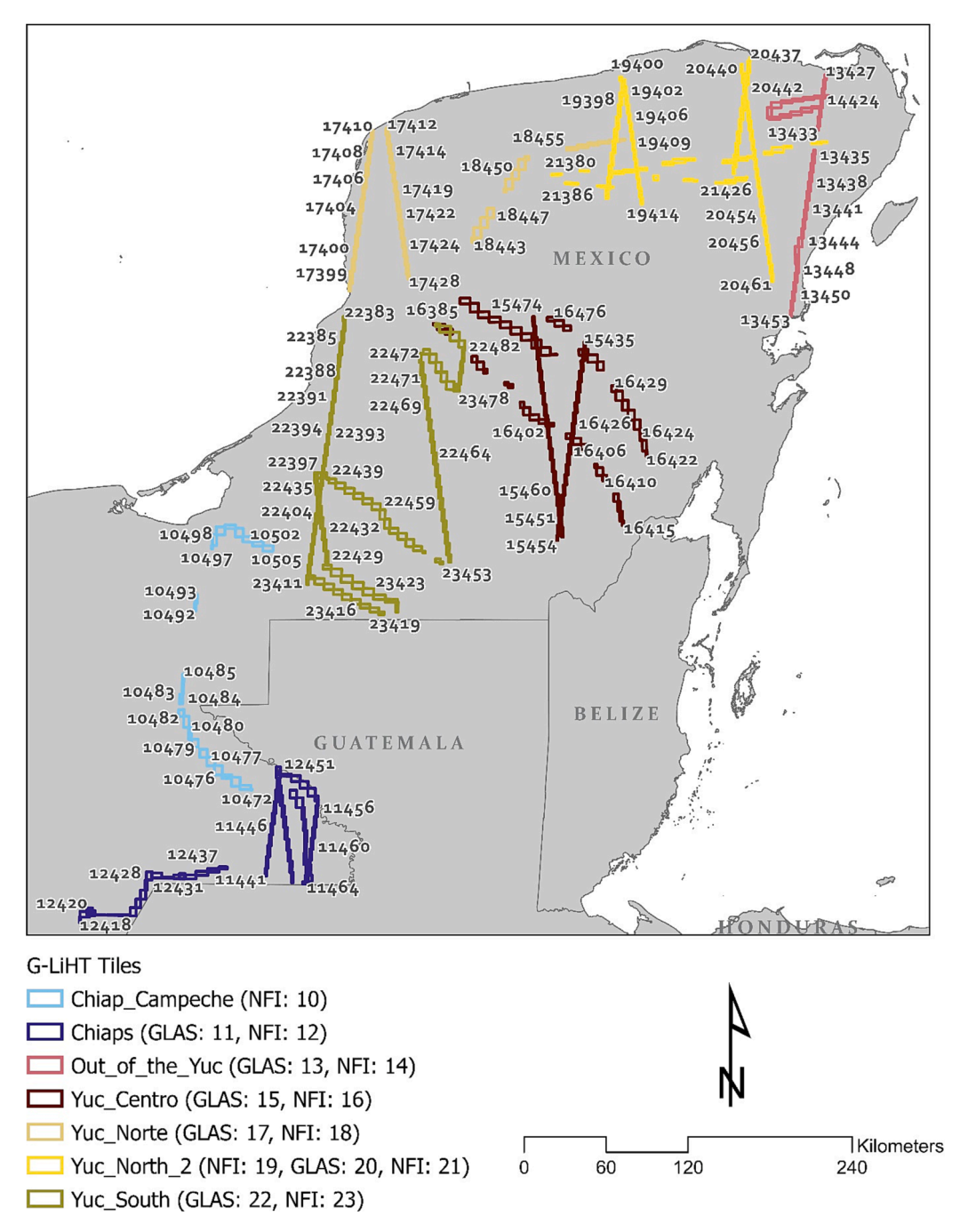


Fig. 1. Map of the Maya lowlands showing the analyzed G-LiHT tiles with unique identifiers based on NASA file names (with the AMIGACarb\_prefix removed). Tiles are color-coded based on flight region, and the two-digit numbers in parentheses refer to the first two numbers in the tile numbers (unique identifiers) shown on the map. For clarity, not all tiles are numbered.

square kilometers. Due to the flight pattern of single transects, the average ground point density varies significantly across the dataset (with a range from 0.3 to 11.0), reported in more detail in a previous publication (Schroder et al., 2020), which may bias results in heavily forested areas, due to the impact of vegetation on ground point density (Inomata et al., 2017; Schroder et al., 2021b). Still, ground point densities are sufficient (at least 1 point per square meter) in the majority of tiles to generate high resolution digital elevation models with cell sizes of 1 square meter or less (Rosenswig et al., 2013, 1497). While limited along its short axis, the full transect presents a significant cross section of the Maya landscape of southeastern Mexico. These data offer a unique opportunity to interpret regional variation across diverse environments, cultural areas, and physiographic sub-regions of the Maya lowlands. Furthermore, as these data were collected without input from archaeologists, the transects cover understudied areas largely distant from known archaeological sites, especially the largest political and urban

We previously reported on the analysis of 458 of the G-LiHT tiles across southesatern Mexico and their environmental context (Schroder et al., 2020). These 458 tiles cover a diverse series of cross-sections of the Maya lowlands, with flight regions including northern Yucatán, southern Campeche and Quintana Roo, Chiapas (including parts of the Eastern Highlands and Lowlands, Central Depression, and Central Plateau), as well as smaller portions of bordering Tabasco and Petén, Guatemala (Fig. 1). Using the previously annotated structure data that had informed estimates of settlement density across the dataset (Schroder et al., 2020), we calculated Gini indices based on structure dimensions. We then contextualized these Gini indices with several cultural and environmental variables previously discussed in other publications, including proximity to known sites, rainfall patterns, and access to resources, including surface water (Golden et al., 2016; Schroder et al., 2020). Some tiles were necessarily eliminated in the present study due to small sample sizes, discussed in more detail below.

A lingering issue with the G-LiHT dataset and the annotated archaeological features is the question of temporality. The data documented in the G-LiHT survey represent a palimpsest and accretion of human occupation and modification of the landscape over millennia, especially given that Maya households periodically expanded their structures over time, both horizontally and vertically. Despite relatively successful attempts to distinguish between Preclassic (1000 BCE-250 CE) and Classic period (250-800 CE) constructions in LiDAR data in defined sub-regions (Garrison et al., 2019), the spatial scale of the G-LiHT data cover a diversity of Maya settlement patterns that resist simple categorization. Furthermore, much of the G-LiHT data record settlement associated with the Colonial period (1521-1821 CE) and later. The present study focuses on regional variation and automation, while future research will require a greater engagement with temporality, through closer visual inspection of the G-LiHT tiles, integration with site-based approaches, contextualization with the culture histories of sub-regions, and ground verification. With these caveats, we highlight regional trends across large portions of the Maya Lowlands, with the goal of refining these results through additional analyses to incorporate the temporal dimension. We note that although the issue of temporality is more pronounced in the G-LiHT data, other LiDAR surveys and sitebased approaches face similar challenges.

The G-LiHT transect data were divided into smaller sample tiles by the original researchers with an average tile length of approximately 7 km and grouped by the labeled flight regions shown in Fig. 1. These data are available at <a href="https://gliht.gsfc.nasa.gov">https://gliht.gsfc.nasa.gov</a>, all beginning with the prefix AMIGACarb\_, followed by the character strings shown in the legend in Fig. 1, GLAS or NFI (referring to the general direction of transects), the month and year of data collection, and ending with a three-digit number. For consistency, we preserve this naming convention, but for data processing we named tiles based on a unique identifier, beginning with the two-digit codes shown in the Fig. 1 legend, followed by the original three-digit number equivalent to each tile. For example, the

AMIGACarb\_Yuc\_South NFI s452 tile shown in Fig. 2 was assigned the value of 23452.

The 7-km length of tiles arguably encompasses a settlement system suitable for the calculation of several variables, including structure density and Gini indices. Researchers in the Belize Valley and Palenque regions, for example, have noted regularly-spaced population centers at similar intervals (Driver and Garber, 2004, 289; Liendo Stuardo et al., 2014; Liendo Stuardo and López Bravo, 2006, 434). Subsequent analyses can assess variability within G-LiHT tiles, but as a first step we focus on macroregional patterns that emerge from calculations based on the 0.3  $\times$  7 km polygons. We recognize that Gini coefficients calculated from these samples may not be representative of entire archaeological communities or settlement systems (Smith et al., 2014, 321); however, the consistency in the application of this approach across the G-LiHT data is useful for comparative purposes, and further research can assess how sampling affects these results. Further analysis could explore how issues of scale affect Gini coefficients, for example, dividing the data into smaller "kernel" sizes or feature clusters (i.e. archaeological sites) (Golden et al., 2021) or expanding coverage of targeted G-LiHT tiles with additional airborne LiDAR surveys, including the use of unoccupied aerial vehicles (UAV), for example (Schroder et al., 2021a). We recognize that at the current scale, the G-LiHT data underrepresent the largest Maya sites, meaning that the Gini coefficients reported here may be skewed – whether higher or lower will require additional comparisons with site-based approaches. As such, the values reported here are not meant to be interpreted absolutely; rather, the comparison of Gini indices across the G-LiHT dataset is presented as a relative measure to assess regional variation. We expect that combining LiDAR datasets like G-LiHT with site-based approaches will improve an overall understanding of Maya landscapes and settlement alongside social inequality.

#### 4. Methods

In this section, we present our methodology for calculating and comparing Gini coefficients used in this analysis. First, we discuss the architectural metrics adopted in this study that were later used in the calculation of Gini coefficients. Second, we explain how features were filtered and selected for this analysis, based primarily on structure and patio size thresholds to include only domestic architecture. Third, we review the methodology for the calculation of architectural metrics based on previously annotated features. Fourth, we acknowledge some of the complications in the automation of our approach. Finally, we present the methodology for the automation of the calculation of Gini coefficients across the large G-LiHT dataset.

In the interest of comparison with other studies, we adopted the methodology outlined by Amy Thompson and colleagues (2021b) to calculate Gini coefficients based on architecture. Six separate Gini indices were calculated in six different ways, based on: 1) structure footprint area, 2) structure volume, 3) patio group footprint area (including the patio), 4) patio group volume (including the patio), 5) footprint area of all structures within patio groups (excluding the patio itself), and 6) volume of all structures within patio groups (excluding the patio itself). This methodology is visualized by Thompson and colleagues (2021b, 9), and results for a portion of one G-LiHT tile are shown in Fig. 2. Each of the six Gini indices represents a different type of differentiation or inequality (Chase, 2017; Peterson and Drennan, 2018); therefore, we present a summary of statistics from each method while focusing primarily on structure footprint area for subsequent analyses.

Given the diverse range of structures present in the sample area, we refined our sampling strategy to focus on only those structures that we believe are most closely associated with individual households and household wealth. This required filtering the data in several key ways, based on either the structure or patio footprints. For calculations based on structure footprints and structure volumes, structures with footprints larger than 275 square meters and below 20 square meters were excluded. These thresholds, suggested by Thompson and colleagues

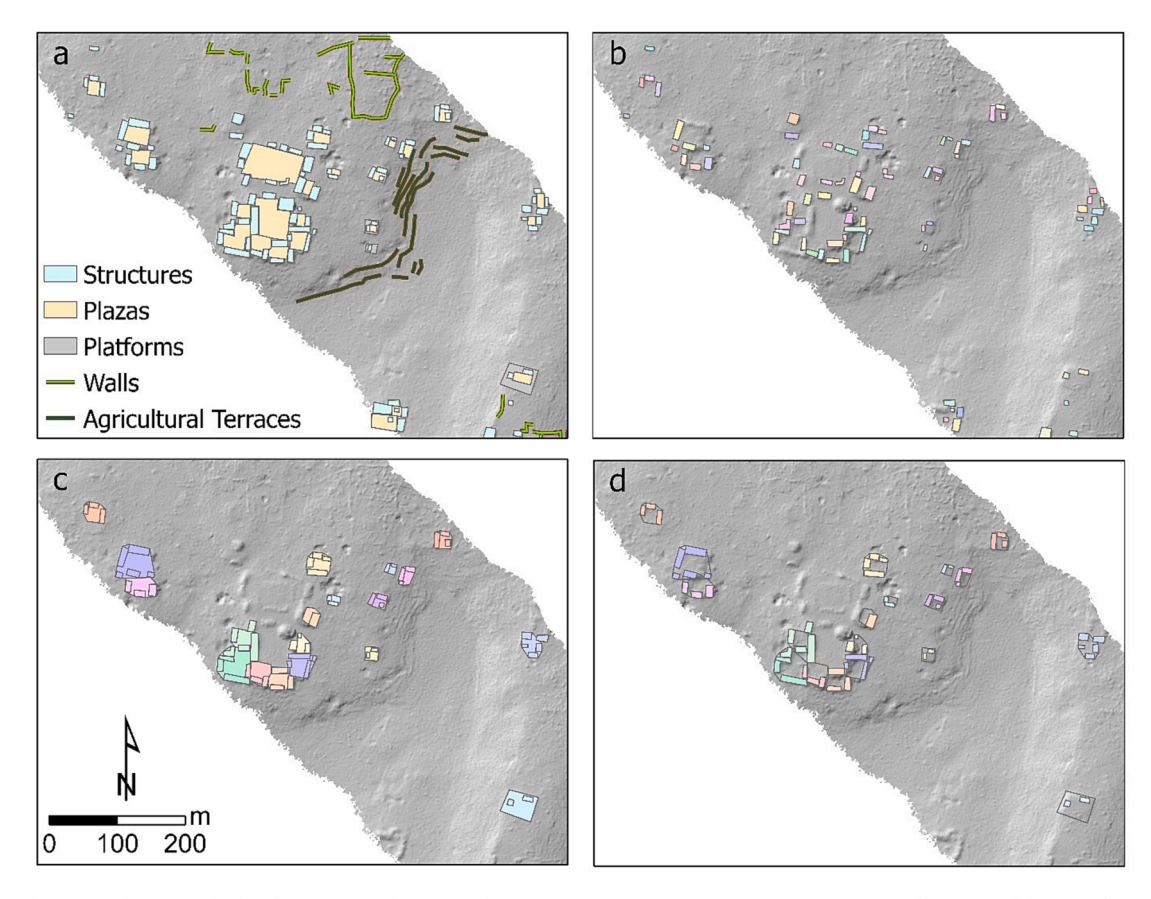
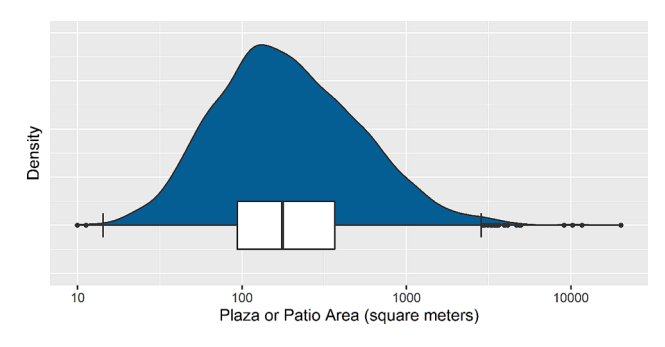


Fig. 2. Subsample of a single G-LiHT flight tile, AMIGACarb\_Yuc\_South NFI s452 (unique identifier 23452), showing a) all annotated features, b) structures used in Gini analysis of structure footprint area and volume, c) patio groups used in Gini analysis of patio group footprint area and volume, and d) structures used in Gini analysis of structure area and volume within patio groups.

(2021b) may require adjustment in future analyses, especially at the lower end, as Wendy Ashmore (1981) cited 20 square meters as an average figure for house mound footprints, rather than the minimum. Average house mound footprints and the necessary thresholds for the calculation of Gini indices will vary across regions. Still, when relying on regional comparisons of LiDAR, adopting a lower cutoff can minimize false positives and ambiguous features; in fact, Scott Hutson and colleagues (2021) suggested a higher cutoff for minimum building size (50 square meters) when identifying house mounds from the G-LiHT LiDAR data. For patio group footprints, we chose a threshold of 4,000 square meters, described below. Of note, as recommended by Thompson and colleagues (2021b), patio group metrics (both area and volume) include all structures within the patio group (even those below 20 square meters and above 275 square meters).

The data analyzed here are part of a broader long-term study. Previously, feature annotation identified structures, basal platforms, and individual plazas (regardless of size) rather than patio groups. Furthermore, we did not distinguish between large public plazas as discussed by Inomata (2006) and domestic patios in the annotations. In the current analysis, separating large plazas from domestic patios required a threshold based on area. Here, the area of these features was calculated with the Add Geometry Attributes tool in ArcGIS Pro version 2.8.3. Determining patio group footprint area from the annotated features required a decision of which structures within certain distances of plazas would be considered part of the same patio group, an adjacent patio group, or an individual structure, depending on the relative settlement density. In some cases, patio groups and structures were built atop basal platforms, which aided in their identification. In contrast, some platforms, especially those dating to the Preclassic period, can support small structures difficult to identify in LiDAR (Garrison et al., 2023, 283).

However, any platform without discernible superstructures was eliminated from the analysis by restricting the maximum structure footprint area to 275 square meters. To semi-automate the definition of an entire patio group, we adopted the following workflow in ArcGIS Pro: 1) Spatial Join of structures within 10 m of plazas, assigning a target field to structures based on the associated plaza, 2) a manual check of structures joined multiple times (within 10 m of several plazas), followed by a manual assigning of a structure to a plaza when appropriate, 3) Minimum Bounding Geometry based on merged structures and plazas sharing the same target field using the Convex Hull setting, and finally 4) using the Merge tool to combine the results of the Minimum Bounding Geometry with intersecting basal platforms. After a visual check of defined patio groups, we omitted extreme outliers of large, plazaoriented architecture over 4,000 square meters, which represent mixed areas of public, ritual, and administrative architecture at political centers, rather than individual household areas (Fig. 3).



**Fig. 3.** Density plot and box plot (half violin plot) showing the distribution across the G-LiHT dataset of plaza or patio sizes on a logarithmic scale.

Calculating the volume of features is less straightforward than calculating their footprint area and additionally necessitates access to a high-resolution digital elevation or terrain model (DEM/DTM); in our case, features were previously identified with raster derivatives (hillshade) of DEMs produced from the point clouds collected by the G-LiHT study. Without access to DEMs, feature volume could theoretically be estimated if the height is known using cubic solid calculations (e.g., rectangular prisms, cones, etc.) (Lacquement, 2010; Magnani and Schroder, 2015). To calculate volume of features, we modified a method developed by Adrian Chase and colleagues (forthcoming) that 1) extracts the point coordinates from the vertices of features, 2) interpolates a DEM between these vertices (a hypothetical ground surface underneath features), 3) subtracts the interpolated, hypothetical DEM from the archaeological DTM, 4) multiplies the result by the horizontal resolution of the DTM, then 5) uses Zonal Statistics to sum the resulting cells assigned to each feature class. Our modification altered step 3 by creating a conditional evaluation to remove negative values, so that in step 5 only positive values would be summed. We incorporated this script into a model in ArcGIS Pro that iterated through the folders that contained the raster DEMs of all G-LiHT tiles analyzed in the present

Semi-automation was not perfect, however, and aside from the visual checks already mentioned and the reassignment of certain features to appropriate patio groups, some of the volume calculations returned false estimates. For example, the interpolation of feature vertices that fell outside of the corresponding G-LiHT tile returned elevation values and volume estimates that were too large. These features were either removed or redrawn manually. In addition, features that were improperly annotated also resulted in excessive volume estimates. Such outliers were manually removed from the analysis.

Sample sizes also vary significantly from metrics comparing structures to plazas because the study area contains fewer plazas than structures (each plaza will often have 2 or more structures). Additionally, due to the manner of feature annotation based on a visual analysis of DEMs, plazas were only identified when evidently sunken or raised, or when clearly defined by the orientation of structures on at least 3 sides (Schroder et al., 2020). Many plazas, therefore, were likely left unmarked because of the variable resolution of the data and when structures were harder to distinguish, especially in lower density settlement without sufficient contextual clues. Without systematic ground verification across the dataset, any calculations based on plazas will be speculative.

Because of the complications in defining patio groups, which requires better consideration of regional variability in form and ground verification, we chose to focus on Gini indices calculated from structure footprint area for this analysis. Structure footprint area is more complete in the annotated G-LiHT data considered here. Namely, 75 of the analyzed G-LiHT tiles include structures without plazas, so we are able to include more data by analyzing structures rather than patio groups. For comparative purposes, we recommend calculating Gini coefficients using several lines of evidence, but other researchers should determine the appropriate metrics based on the regional, cultural, and ecological contexts of their datasets.

Once calculated in ArcGIS Pro, area and volume figures were matched to the value of their relevant G-LiHT tile, based on their features' centroids. Each G-LiHT tile was assigned a unique identifier based on flight region and the 3-digit value already stored in its file path (Fig. 1). Feature data were exported as a single comma separated values (.csv) table consisting of 2 columns, where each row represented a feature, with a unique identifier column and a geometry metric column. These data were then imported as a data frame to R, where the Gini function from the DescTools package was applied to grouped data based on the unique identifier, with statistics for each unique identifier or G-LiHT tile output to a new data frame. To advance open science and the utility of these research methods, the code used in this analysis is made publicly available (https://github.com/whitschroder/Gini-automatio

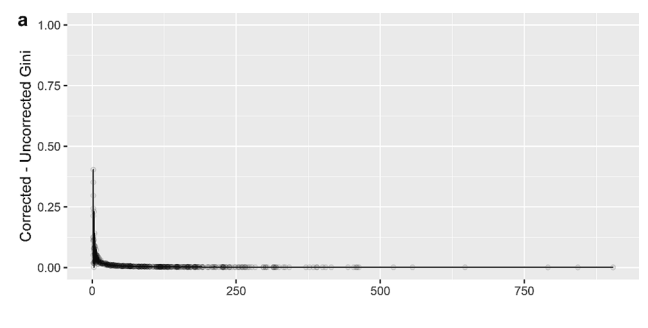
n). G-LiHT data are available through NASA (https://gliht.gsfc.nasa. gov). The code used in this study could be applied to any dataset where archaeological features have been assigned to a unique value (for example, a series of archaeological sites, regions, districts, or samples). Results were then imported back into ArcGIS Pro and joined (Join Field tool in ArcGIS) to a G-LiHT tile's environmental and archaeological data previously compiled and reported (Schroder et al., 2020). When linked to this previously compiled data, each tile's Gini coefficient was then compared to its environmental and cultural variables, including distance to known archaeological sites (Witschey and Brown, 2010), distance to surface water (INEGI, 2000), settlement and feature density (Schroder et al., 2020), and rainfall and seasonality of precipitation expressed as the coefficient of variation of monthly rainfall (Fick and Hijmans, 2017, https://www.worldclim.org). These variables were selected due to their availability, relationship to known archaeological contexts and core ecological contexts identified in a preliminary study (Golden et al., 2016), and because a follow-up analysis identified these socioenvironmental variables as the most closely correlated with settlement density in the study area (Schroder et al., 2020).

#### 5. Results

Several authors have noted the need for robust samples when calculating and interpreting Gini coefficients, observing that lower sample sizes tend to underestimate the Gini index while increasing the difference between upper and lower limits of the confidence interval (Bowles and Carlin, 2017, 2; Peterson and Drennan, 2018, 41). Larger samples will narrow the confidence interval, as additional data are unlikely to affect results significantly. The G-LiHT data analyzed in this study presented a valuable opportunity to test the effects of sample size on Gini coefficients.

Out of 458 sample tiles, the number of structures per tile ranged from 0 to 1,076, while the number of plazas per tile ranged from 0 to 97. Calculating Gini coefficients from structure area and volume, therefore, provided higher sample sizes. In an exercise to compare how sample sizes affect the results of the Gini coefficient calculation, we first filtered G-LiHT tiles to include only those with two or more structures (at least 2 values are necessary to calculate a Gini index) with footprint areas between 20 and 275 square meters resulted in a total of 393 G-LiHT tiles. The uncorrected (biased) and corrected (unbiased) Gini coefficients based on structure footprint area were calculated for each tile, and the difference between these values was plotted against the sample size of structures per G-LiHT tile (Fig. 4). The results show that the lowest sample sizes can increase the corrected Gini coefficient by a value of more than 0.4 compared to the uncorrected value. This bias is largely eliminated with sample sizes of 10 or higher, where the difference between uncorrected and corrected Gini indices amounts to less than 0.05. The confidence intervals for smaller samples had a wide range of values (at a 95% confidence level), with the largest range between upper and lower Gini coefficients reaching higher than 0.8 with a sample size of 2. Above a sample size of 10, the highest confidence interval range is less than 0.3. We found that sample sizes of more than 100 were necessary to reach confidence interval ranges below 0.1. Based on this exercise, we therefore opted to limit our study to G-LiHT tiles with 10 or more features (structures or plazas), and all subsequent findings presented here are based on this sample size (Fig. 5). Other researchers should determine appropriate sample sizes based on their own data, although our findings may provide a guideline. By adopting a sample size of 10 in this study, we attempt to minimize the effects of the limited horizontal spatial coverage of the G-LiHT tiles.

Quantiles of analyzed data are presented in Table 1. Across the dataset, corrected Gini coefficients range from as low as 0.12 (based on patio group area) to 0.82 (based on structure volume within patio groups). As Adrian Chase (2017, 37) has cautioned, Gini indices generated from different metrics should not necessarily be assumed to represent the same type of inequality; in the present study Gini indices



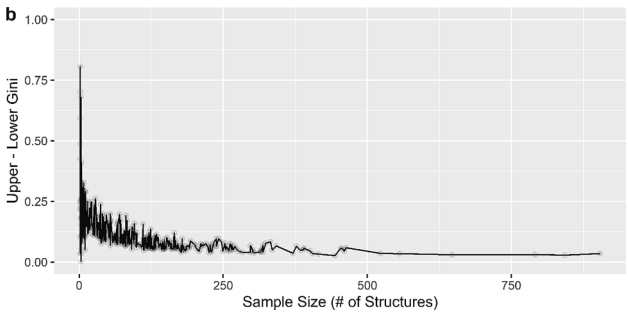


**Fig. 4.** Effect of sample size on a) difference between corrected and uncorrected Gini coefficients based on structure footprint area and b) upper and lower confidence intervals of Gini coefficients based on structure footprint area.

varied significantly depending on the metric used. In some cases, when Gini coefficients calculated from distinct metrics differ significantly, the data may be demonstrating several kinds of differentiation (or inequality) that are worth investigating further (Peterson and Drennan, 2018, 54). We divided the distribution of Gini coefficients calculated from each metric into 5 quantiles, shown in Table 1 alongside structure densities and sample sizes. A clear pattern emerges that Gini coefficients tend to increase across the table columns from left to right, with the lowest Gini indices calculated from structure footprint area (ranging from 0.14 to 0.45) and the highest based on the volume of structures within patio groups (ranging from 0.24 to 0.81) (Fig. 6). Notably, dispersion also increases across each metric, with Gini coefficients calculated from structure volume in patio group showing the largest range of values. Due to space constraints, we cannot present Lorenz curves for each of the 6 metrics for each G-LiHT tile, but examples are shown in Fig. 7.

We propose several reasons for the higher Gini coefficients based on volume metrics compared to area values. With some exceptions (Smith et al., 2014), other studies have reported higher values for Gini indices based on volume versus area, especially in the Maya area (Chase, 2017; Thompson et al., 2021b, 14). Volume estimates based on LiDAR or a DEM more than likely include at times the natural topography around and under features. Proper volume estimates require careful annotation of features, often confirmed by ground verification; therefore, while minor annotation errors will not negatively influence footprint area estimates, these same errors could profoundly impact volume estimates, especially in areas of high topographic variation. Many Maya households took advantage of natural topography, and accurate volume estimates require excavation to determine the extent of construction over bedrock. Due to the size of the G-LiHT tiles (averaging approximately 7 km in length), natural topography can vary significantly from upland areas to bajos, or lowlands. As the natural topography affects volume estimates, upland areas with higher volumes will skew Gini coefficients when compared to lowland structures in flat areas. Following the guidelines established by Amy Thompson and colleagues (2021b), for Gini coefficients calculated for individual structures we eliminated structure areas that did not fall between 20 and 275 square meters, but these same structures were included when calculating Gini coefficients

based on patio groups. In addition, all tiles in the current study had fewer than 100 plazas, resulting in small sample sizes for patio group-based metrics, which we have established can contribute to wide confidence intervals. Aside from these observations, we can conclude that across the dataset (and the Maya lowlands in general), higher differentiation exists in plaza form in relation to structure form, and additionally, structure volume is more variable than structure area, based on the higher Gini coefficients generated from these metrics.

In another effort to interpret Gini coefficients based on different metrics, we generated a correlation matrix showing statistically significant positive correlations across all bivariate comparisons (Fig. 8) (correlation coefficients and p-values are included in supplementary materials). This analysis suggests that despite the variation in results based on each architectural metric, the Gini coefficients increase somewhat predictably, and that tiles with high or low Gini coefficients based on one metric tend to exhibit high or low Gini indices based on other metrics, respectively. Furthermore, the relative magnitude of correlation coefficients shows that the strongest correlations are between Gini indices based on similar metrics, for example when comparing areas or volumes of structures and patio groups, or when comparing structure metrics or patio group metrics. Predictably, a strong correlation exists between the indices generated from patio group area and patio group structure area, as larger patio groups tend to have more structures and higher structure footprint areas. Still, discrepancies in the comparisons are due to the methodological challenges discussed above and the fact that such measurements of differentiation are distinct though related. We believe that including the additional vertical dimension of structures adds more uncertainty, and although Smith and colleagues (2014) suggest that the verticality of Mesoamerican architecture might be more relevant than area when assessing inequality, we opt to focus on structure area in this study. Presently, we are less concerned with the absolute values of the Gini coefficients presented here and more interested in the relative values and trends across the study

In a previous analysis, we calculated and presented settlement density across the 458 G-LiHT tiles analyzed (Schroder et al., 2020), and the resulting categorical quantiles of these data are also presented in Table 1. In the same analysis, we compared settlement density to several environmental variables. Here, we expand this study to include a comparison of these environmental variables alongside Gini coefficients. Due to space constraints and the limitations of calculating Gini indices based on patio groups and volumes, we focus only on Gini coefficients calculated from structure footprint area, although we have established correlations between each metric. The comparisons between previously identified environmental variables such as rainfall and seasonality, settlement density (Schroder et al., 2020), and Gini coefficients are shown in the correlation matrix in Fig. 9. While correlations between structure density and distance to Type 1 or Type 2 site, terrace density, rainfall, seasonality, and distance to surface water are statistically significant (at p less than 0.05), these results indicate statistically insignificant, weak positive correlation between Gini coefficients and these same variables, including settlement density, meaning that Gini coefficients do not necessarily increase linearly relative to structure density. In other words, denser, more urban settlements in the study area are not necessarily characterized by higher differentiation in structure size. Amy Thompson and colleagues (2021b) reached a similar conclusion in their comparison of sites in southern Belize with Chunchucmil, Caracol, Uxul, Palenque, and Tikal. Still, the tiles with the highest feature densities generally have the highest Gini coefficients, while more variability is present in lower density tiles. Gini indices, however, cluster between 0.2 and 0.4 despite feature density. In addition, when separated by flight region, some areas show stronger trends between Gini coefficient and settlement density, notably the AMIGACarb Yuc Norte, AMIGA-Carb Out of the Yuc, and AMIGACarb Chiaps tiles, although these results are not statistically significant (Fig. 10) (correlation coefficients and p-values are included in supplementary materials).

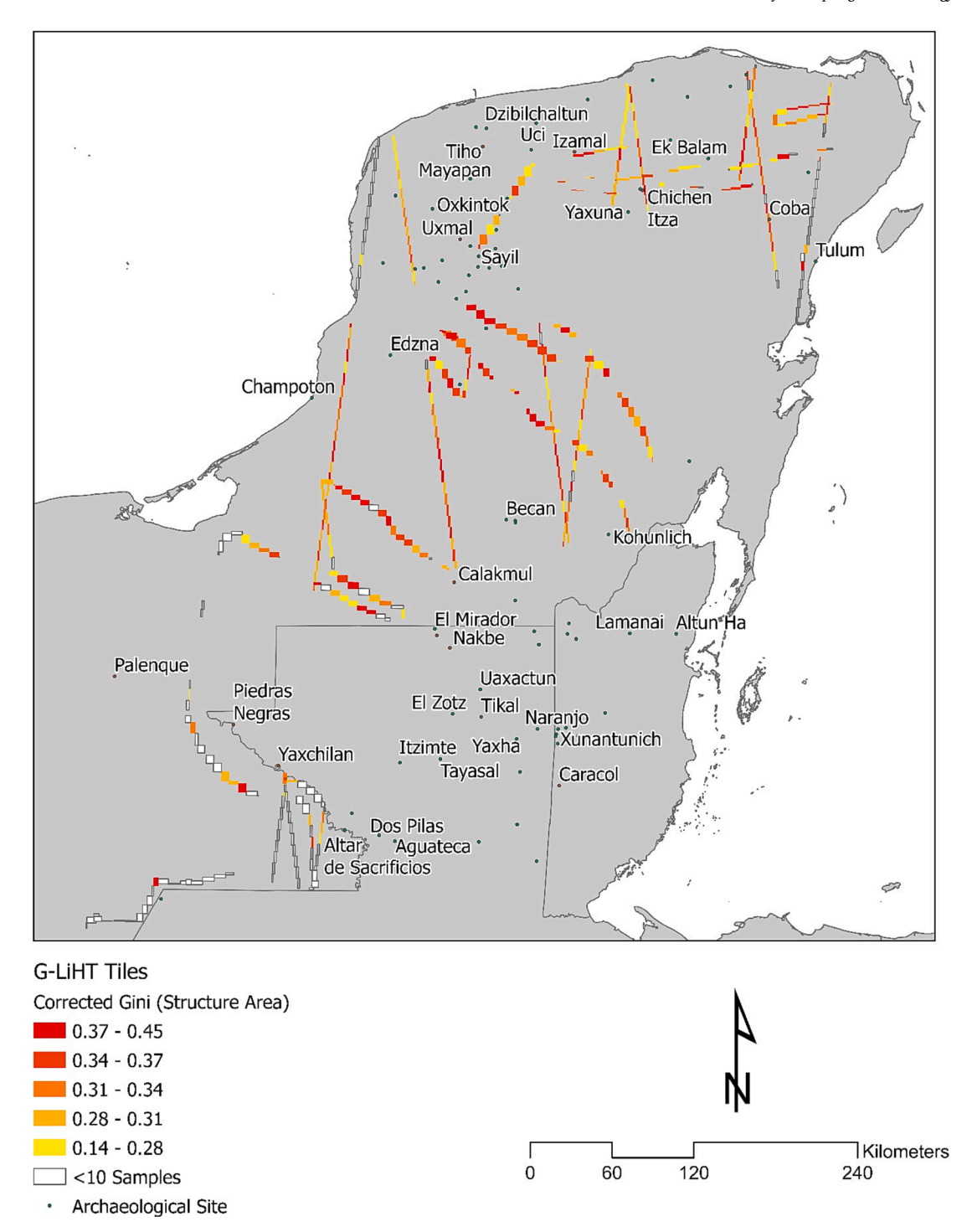


Fig. 5. Map of the Maya lowlands showing Type 1 and 2 archaeological sites (Witschey and Brown, 2010) and the analyzed G-LiHT tiles, color-coded to the corrected Gini coefficient based on structure footprint area quantiles shown in Table 1.

A related comparison is the relationship between a tile's Gini coefficient and its distance to known urban centers or large sites. Here, we rely on the Walter Witschey and Clifford Brown (2010) electronic atlas of Maya settlement. Despite flaws and inconsistencies in the data, the largest – typically well-documented – archaeological sites (classified as Type 1 and Type 2 in the dataset) tend to be placed with reasonable accuracy. Notably, the correlation matrix in Fig. 9 shows no significant linear correlation between a G-LiHT tile centroid's distance to the nearest Type 1 or Type 2 site and its Gini coefficient. In contrast, as noted earlier, we have established a negative correlation between settlement density and distance to Type 1 or Type 2 site, meaning that

settlement density increases with proximity to large sites (Schroder et al., 2020). Yet clearer patterns emerge when data are separated by flight region, showing that Gini coefficients across regions tend to decrease as distance to large sites increases (Fig. 11). Of note, the only flight region with a statistically significant (p less than 0.05) negative correlation between Gini coefficients and distance to Type 1 or Type 2 sites is the Yuc\_Centro flight region (correlation coefficients and p-values are included in supplementary materials).

Other weak relationships are shown between Gini coefficients and agricultural terrace linear density (positive), rainfall (negative), and seasonality (positive); however, these results are not statistically

**Table 1**Feature density and corrected Gini coefficients by G-LiHT tile divided into 5 quantiles.

Quantile	Structure and Platform Density per Ha	Gini Coefficients					
		Structure Area	Patio Group Area	Structure Area in Patio Group	Structure Volume	Patio Group Volume	Structure Volume in Patio Group
Highest 20%	0.93-3.75	0.37-0.45	0.45-0.60	0.47-0.60	0.59-0.79	0.69-0.81	0.67-0.82
Higher	0.52-0.93	0.34-0.37	0.41-0.45	0.41-0.47	0.55-0.59	0.60-0.69	0.61-0.67
Middle	0.21-0.52	0.31 - 0.34	0.36-0.41	0.35-0.41	0.52 - 0.55	0.55-0.60	0.52-0.61
Lower	0.02-0.21	0.28 - 0.31	0.30-0.36	0.29-0.35	0.48-0.52	0.47-0.55	0.45-0.52
Lowest 20%	0-0.02	0.14-0.28	0.12 - 0.30	0.19-0.29	0.26-0.48	0.33-0.47	0.24-0.45
Sample Size (# of Tiles)	458	333	126	126	332	126	126

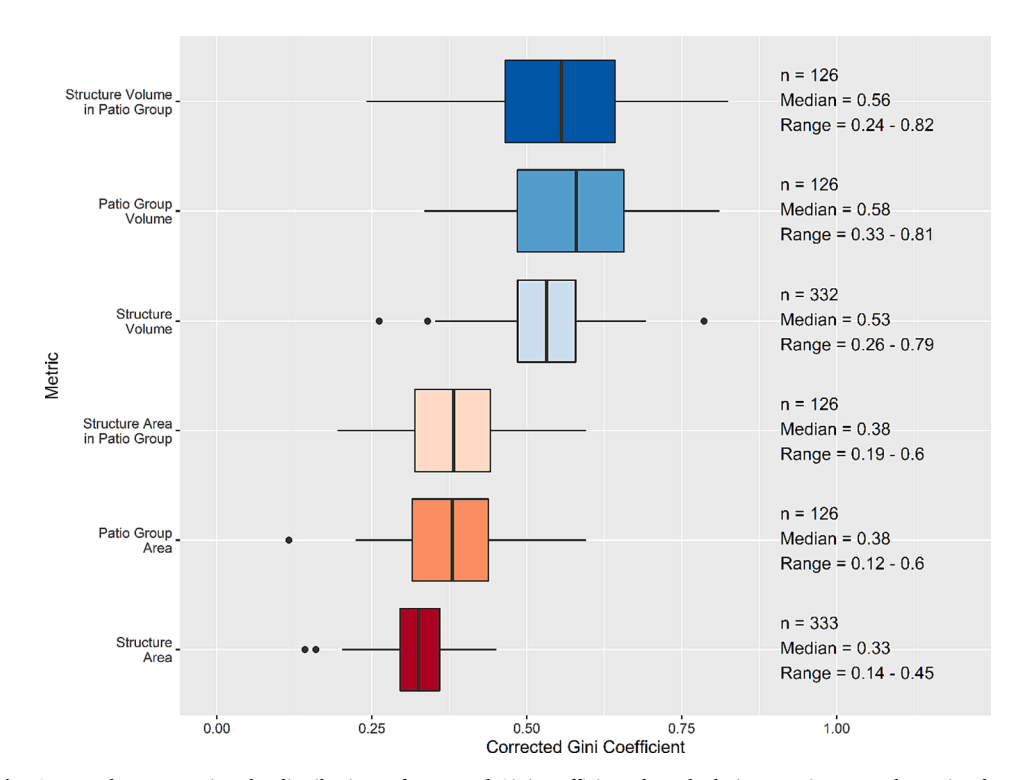


Fig. 6. Box plots comparing the distributions of corrected Gini coefficients by calculation metric across the entire dataset.

significant, complicating the potential to understand the relationship between access to resources and inequality. As trends, Gini coefficients seem to increase in relation to the density of agricultural intensification in the form of terracing. Furthermore, as rainfall decreases and seasonality increases. Gini coefficients increase - could more variable access to water be reflected in higher Gini indices? Yet, no significant linear correlation exists between distance to surface water and Gini coefficients – perhaps in future studies, access to subsurface water could be incorporated into this analysis. Such analyses could be paired with other studies, such as agricultural capability drawn from soil maps. We present these results merely as observations for future work, but the takeaway is that correlations between settlement density and these chosen environmental variables are not matched by comparisons with Gini coefficients, shown in Fig. 9 and discussed in more detail by Schroder and colleagues (Schroder et al., 2020). The values of these Gini coefficients (and perhaps inequality) do not follow the same patterns across the Maya landscape as does settlement density.

Another goal of this study is to compare the nature of settlement across subregions of the Maya lowlands. The simplest approach is to use the flight paths of the LiDAR scans, classified into 7 flight regions, from north to south, Yuc\_Norte, Yuc\_North\_2, Out\_of\_the\_Yuc, Yuc\_Centro, Yuc\_South, Chiap\_Campeche, and Chiaps. Fig. 12 shows the distributions of settlement density and Gini coefficients by flight region.

Although the highest Gini coefficients between 0.37 and 0.45 appear across the dataset, the largest concentrations of the highest Gini values occur in the Yucatán Centro NFI, Yucatán South GLAS, and Yucatán South NFI transects, corresponding with the Central Lowlands of southern Campeche and Quintana Roo. These same data suggest marked differences between settlement density and Gini coefficients in Highland Chiapas and its foothills compared to other portions of the Central and Northern Lowlands.

We suggested previously that much of the variation in feature distribution across the G-LiHT dataset of southeastern Mexico can be better understood in relation to the physiographic sub-regions defined by Timothy Beach and colleagues (2015) (Fig. 13). When each tile is assigned one of the 17 physiographic sub-regions encompassed by the study area based on the tile's centroid, some clearer patterns emerge. Despite some differences, the majority of physiographic sub-regions show a similar distribution, with medians hovering between Gini coefficients of 0.3 to 0.35. The North Coast, however, shows a smaller median, while the Puuc-Bolonchen Hills and Edzna-Silvituk Trough exhibit higher medians. The results from the Puuc hills and adjacent sub-regions again raise issues surrounding the verticality of architecture, and furthermore, the temporality challenge. For example, based on structure area data from Sayil, Strawinska-Zanko and colleagues (2018, 176), attributed a high Gini index (0.71) at the site not to geography but to the

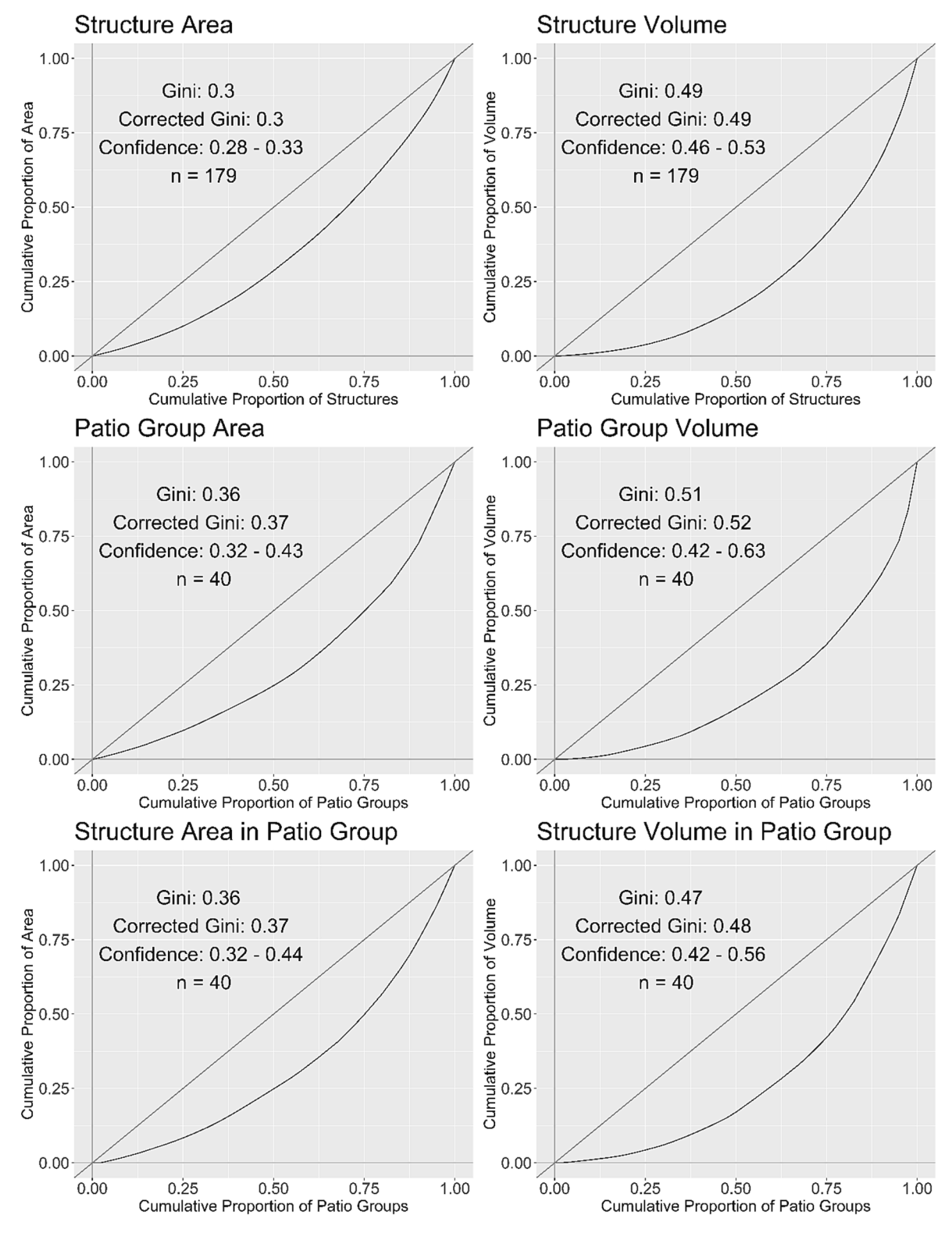


Fig. 7. Lorenz curves of cumulative proportions from the same, single G-LiHT tile (AMIGACarb\_Yuc\_South NFI s452 or unique identifier 23452) shown in Fig. 2 comparing the 6 different Gini metrics.

Terminal Classic period (800–1000 CE) occupation of the region, a time characterized by increasing social inequality.

Smaller data ranges in the Highland Ranges and Valleys, Rio de la Pasion, and Uayamil regions are also notable. Although not shown in Fig. 13 due to small sample sizes, the Caribbean Reef and Eastern Coastal Margin and Chiapas, Grijalva River regions also exhibit lower Gini coefficients. These findings suggest regional patterns in the distribution of

inequality across the Maya lowlands, with several key exceptions, notably representing the northwestern, southwestern, and eastern geographic extremes of the study area. These sub-regions are the most peripheral parts of the Maya lowlands, and they are additionally located in resource rich coastal and riverine environments where inequality may be reduced (Glover and Rissolo, 2023; Rogers et al., 2011). Such physiographic sub-regions may generally have more widely dispersed and

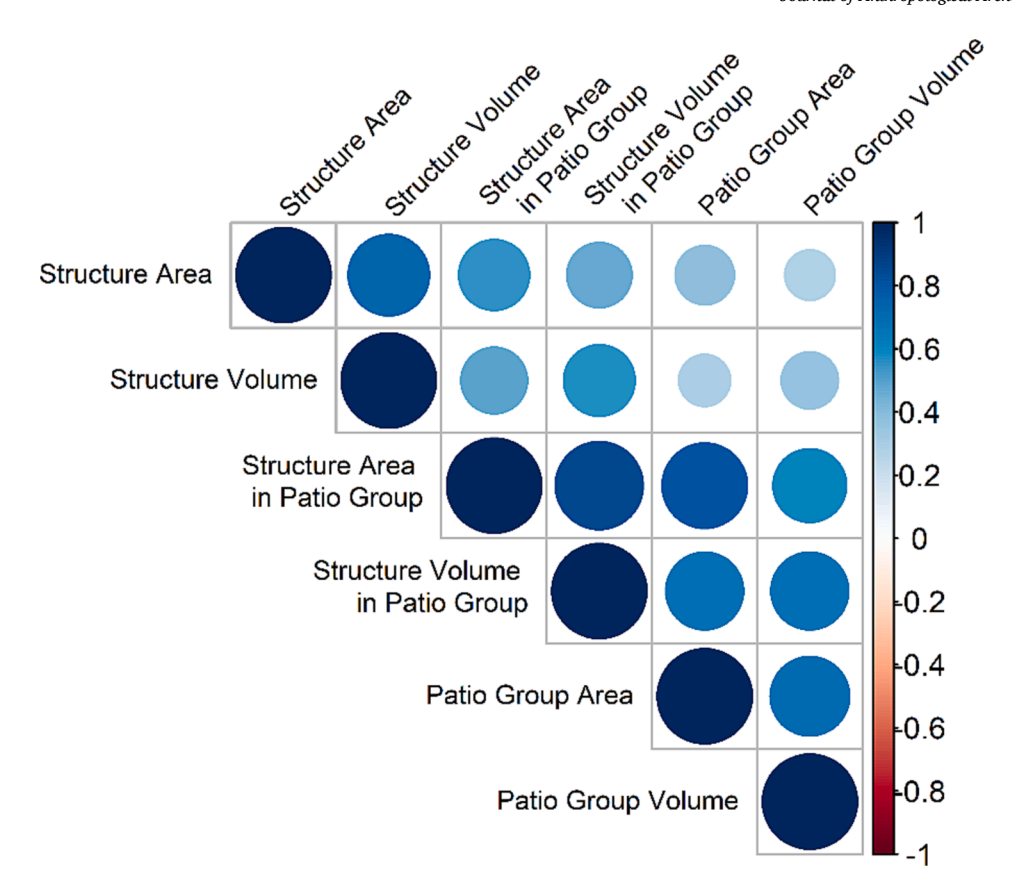


Fig. 8. Correlation matrix showing correlations between corrected Gini coefficient metrics across the entire dataset (only the 126 tiles for which all 6 metrics could be calculated). Correlations range from positive (blue) to negative (red). Color intensity and circle size are proportional to correlation coefficients. (For interpretation of the references to color in this figure legend, the reader is referred to the web version of this article.)

accessible resources, rather than geographically localized resources more readily controlled by individuals or communities.

## 6. Conclusions

In an effort to quantify and measure inequality, archaeologists have adopted economic methods to assess statistical dispersion through the calculation of Gini coefficients. As Christian Peterson and Robert Drennan (2018) observe, archaeologists can calculate Gini coefficients with several lines of data, including house size, agricultural field extent, and artifact assemblages (Munson and Scholnick, 2022). Such lines of evidence are intended as proxies for inequality through more direct measurement of differentiation. Spatial differentiation in Gini coefficients can be used to infer social inequality across sites, and when combined with temporal data, changes in wealth inequality can be traced over time (Kohler et al., 2017).

We explored the possibility of such an analysis at a landscape scale, calculating Gini coefficients based on the scale of the built environment in the form of structures and patio groups annotated from LiDAR terrain data collected by the NASA G-LiHT system over southeastern Mexico. While the results presented here serve as a first step to interpret regional differentiation across the Maya lowlands, they suggest that a landscape approach could offer important context to traditional site-based studies. We can also begin to identify some key findings and patterns in the G-LiHT dataset that will be useful to compare with future analyses of social inequality in the Maya area.

First, we can generalize that across the G-LiHT dataset of southeastern Mexico, Gini values calculated from structure footprint area are typically low. All uncorrected Gini values based on structure footprint area are under 0.5, which is consistent with other values calculated in Mesoamerica and the New World (Kohler et al., 2017; Smith et al., 2014). Furthermore, 20% of all tiles analyzed exhibit Gini coefficients under 0.28. Incorporating the additional height dimension to compare architectural volume profoundly affects the calculation of Gini indices in this study. Aside from possible methodological issues we have discussed, this discrepancy highlights important differentiation in architectural form across the Maya lowlands (Peterson and Drennan, 2018). Future studies of inequality might compare the values of a topographic position index to determine possible correlations between architectural volume, height, and relative prominence with inequality metrics.

Based on the G-LiHT data Gini coefficients, we can identify trends in higher values in areas of higher density of settlement, but regional variation is an important factor. Only in the Yuc\_Centro flight region do Gini coefficients show a statistically significant correlation with distance to larger political centers, perhaps highlighting distinct differences between the Central Lowlands and more peripheral areas of the Maya lowlands. In our 2020 study, we determined that proximity to known sites was a variable associated with higher settlement density. Using the Witschey and Brown (2010) dataset of Maya site locations, we found that 59% of the highest settlement density tiles were located within 10 km of Witschey and Brown's (2010) Type 1 and Type 2 sites, generally corresponding with the largest known archaeological sites in the Maya lowlands. Gini coefficients, however, do not follow a clear pattern when compared to distance from Type 1 or Type 2 sites, although separating the data by region points to areas where future research might be beneficial, particularly in the Central Lowlands. These patterns may reflect the presence of seasonal field houses across the landscape that might explain the clearer correlation between settlement density and proximity to known sites compared to weaker correlations between Gini coefficients, structure density, and distance to large centers (Garrison et al., 2016; Kohler, 1992; Taschek and Ball, 2003). Variable manifestations of differentiation or inequality across the landscape may also

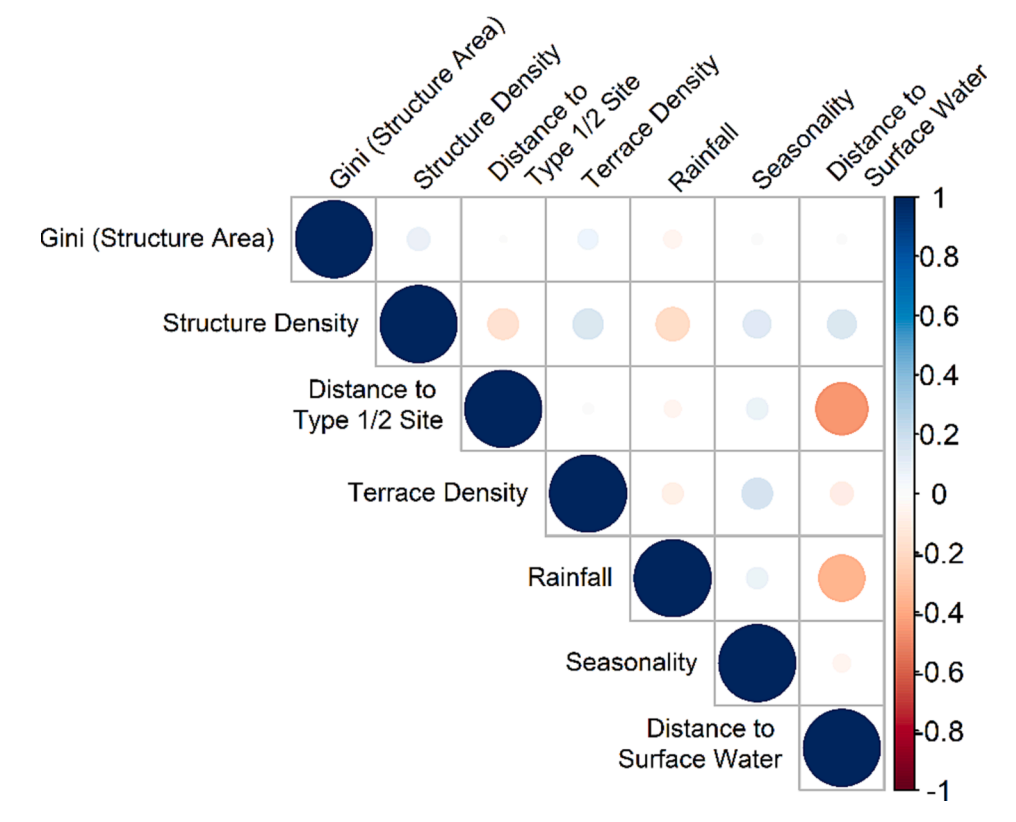


Fig. 9. Correlation matrix showing correlations between corrected Gini coefficients across the entire dataset (only the 333 tiles with 10 or more structures) based on structure area and other variables. Correlations range from positive (blue) to negative (red). Color intensity and circle size are proportional to correlation coefficients. (For interpretation of the references to color in this figure legend, the reader is referred to the web version of this article.)

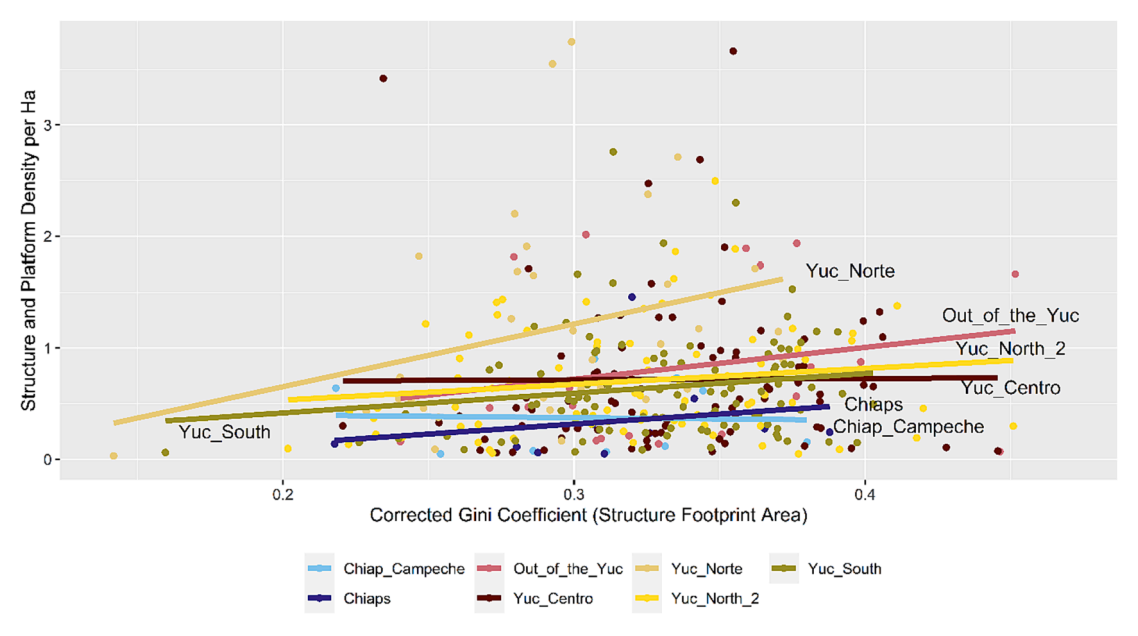


Fig. 10. Scatter plot comparing Gini coefficients based on structure area to structure and platform density by G-LiHT tile, color-coded to flight regions shown in Fig. 1.

point to the decentralized nature of Maya economies (Golden et al., 2020). Generally weak correlations between settlement density and Gini coefficients may also relate to other observed characteristics of low-density urban Maya settlements, for example, that population growth did not necessarily lead to denser cities as predicted by settlement scaling theory (Hutson et al., 2023; Smith et al., 2021).

We are still assessing agricultural intensification across the G-LiHT

dataset of southeastern Mexico, but current findings point to a weak correlation between Gini coefficients and agricultural terrace density. Further studies will examine land tenure in the context of agricultural intensification identified in the G-LiHT data (Barnard, 2021; LeCount et al., 2019; Thompson and Prufer, 2021). Manus Midlarsky (1999), for example, has related the emergence of inequality to land scarcity in agrarian societies alongside population growth (Boserup, 1965;

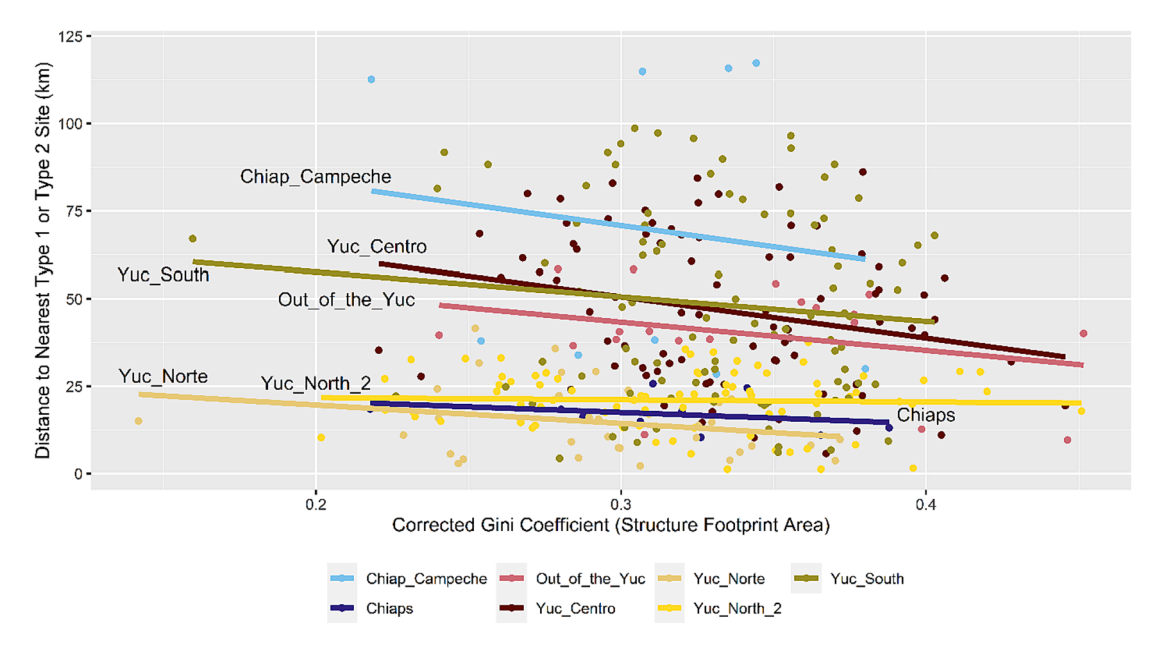


Fig. 11. Scatter plot comparing G-LiHT tiles based on distance to the nearest Type 1 or Type 2 site and corrected Gini coefficients based on structure footprint area, color-coded to flight region.

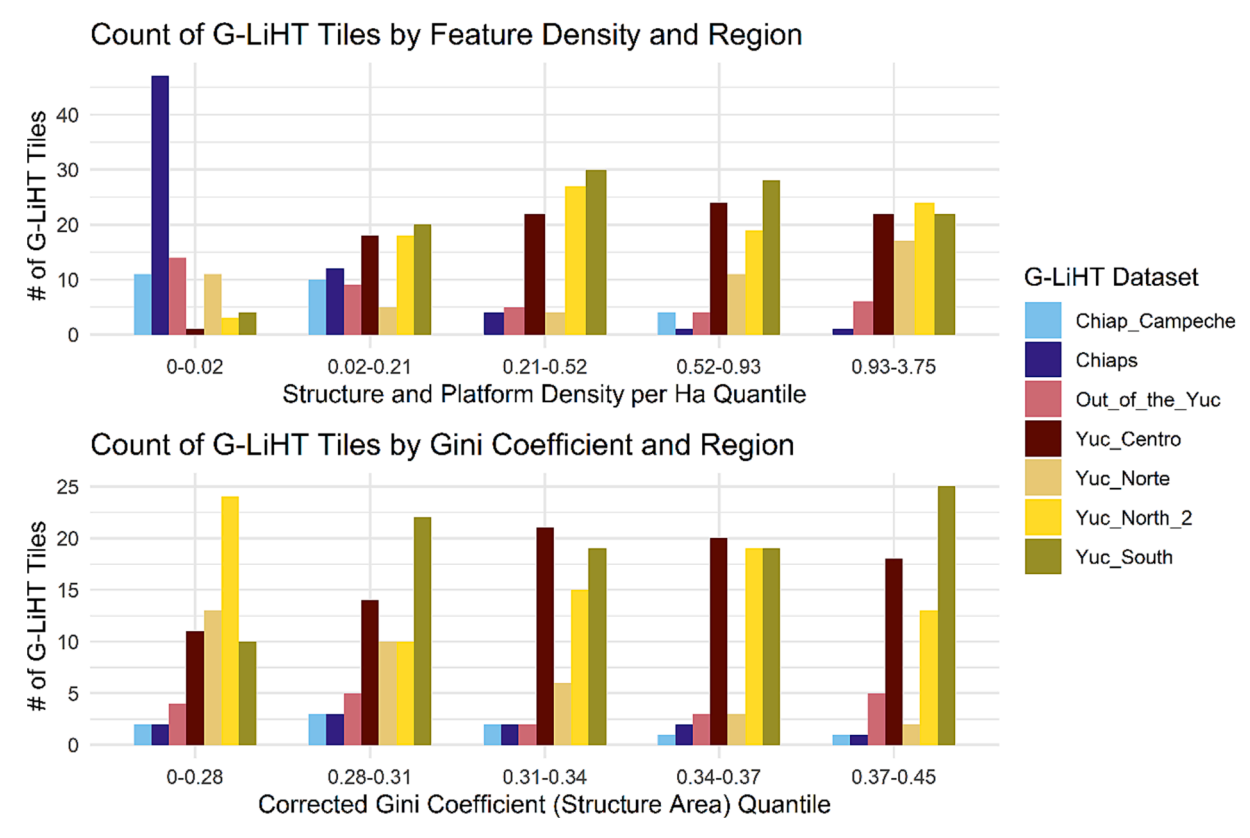


Fig. 12. Bar plots showing the count of G-LiHT tiles by feature density, corrected Gini coefficient based on structure area, and flight region.

Strawinska-Zanko et al., 2018, 165). In this interpretation, the presence of landesque capital to improve land and increase agricultural yield over a limited area should correlate with settlement density and Gini coefficients. Our preliminary results, however, do not reveal clear patterns. While the tiles with the highest density of agricultural terraces have the highest Gini coefficients above 0.3, the majority of tiles with Gini coefficients above 0.3 have low densities of agricultural terraces. Regional variation in agricultural terracing likely contributes to this

weak correlation between agricultural intensification and Gini coefficients. Access to agricultural resources, alongside the evidence presented here on rainfall and seasonality, provides an important path to pursue in future calculations of Gini indices to interpret inequality. Additional studies could assess intensification through field channeling, and agricultural capability using soil maps, and other similar indices to map inequal access to agricultural landscapes.

Clearer patterns emerge when the data are separated by

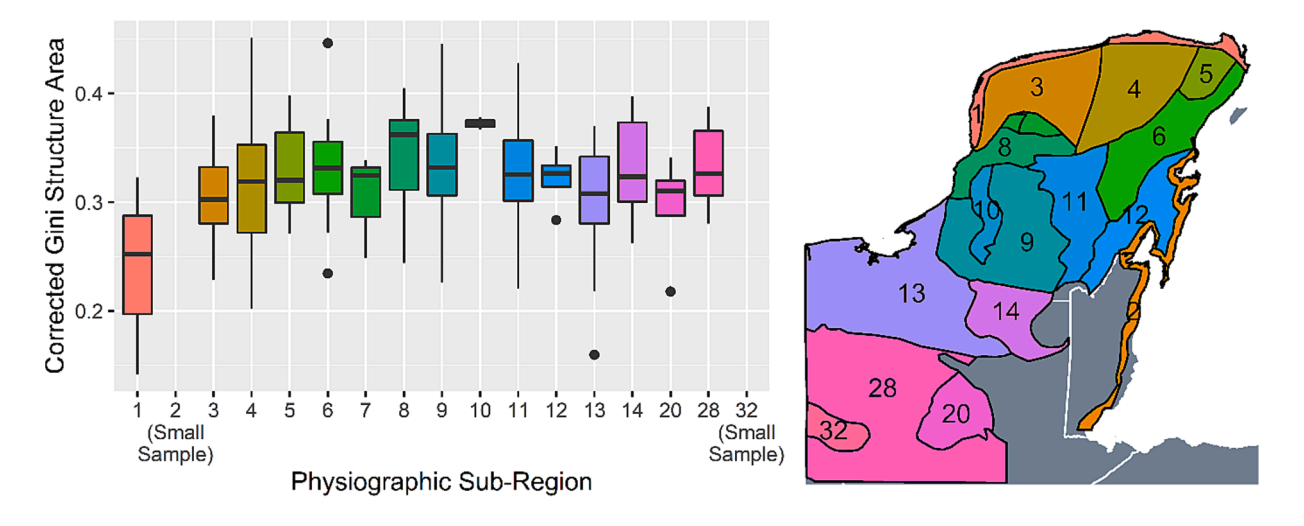




Fig. 13. Box plots showing the distribution of Gini coefficients classified by physiographic sub-regions.

physiographic sub-region. The distribution of Gini coefficients by sample tile is similar across all defined physiographic sub-regions, except in several key areas of Chiapas, the Pasión River, and the North Coast. The peripheral and resource rich locations of these regions may contribute to the lower Gini coefficients that we have presented. Expanding on this landscape and regional scale analysis, comparison of Gini coefficients alongside access to natural resources, likely trade routes, and least cost paths might be beneficial (Thompson et al., 2021a).

Finally, the results of the present study can inform ongoing site-based analyses of Gini coefficients in the Maya area. Thompson and colleagues (2021b, Table 5) provide a useful summary of Gini coefficients across Mesoamerica. Some of the G-LiHT tiles, especially those in the northern Yucatán are near archaeological sites where researchers have calculated Gini coefficients, with better control for temporality. For instance, Clifford Brown and colleagues (2012) report a Gini coefficient of 0.32 for Mayapan and 0.71 for Sayil based on structure footprint area. The value for Mayapan is consistent with results from the G-LiHT data in the Northwest Karst Plain (Yuc\_Norte NFI), where the tile with the highest value results in 0.34 (approximately 4 km to the northeast of the Mayapan site center), while the Gini coefficient for Sayil is notably high. Although none of the G-LiHT tiles exhibit such high Gini coefficients based on structure area on par with that of Sayil, data from the physiographic regions of the Puuc-Bolonchen Hills and the adjacent Central Hills represent some of the highest values in the G-LiHT. The discrepancy between Sayil's Gini coefficient and those from nearby areas of the G-LiHT survey is likely due to the G-LiHT samples' avoiding the largest Puuc sites (suggesting in this sub-region proximity to known archaeological centers and urban areas contributes to differentiation in house size), as well as the question of temporality, highlighted by StrawinskaZanko and colleagues (2018) who also discuss the high Gini coefficient for Sayil. Strawinska-Zanko and colleagues (Strawinska-Zanko et al., 2018, 176) also noted a high Gini coefficient for Komchén (0.56 based on structure area). Our findings from the G-LiHT data are also consistent with the figures cited for Chunchucmil (0.34 based on structure area, 0.56 based on structure volume) (Hutson and Welch, 2021; Magnoni et al., 2012). Another site with a high Gini coefficient, Uxul (0.62), is also consistent with relatively higher Gini coefficients from G-LiHT tiles in the southern Campeche sub-region of the Petén Karst Plateau and Mirador Basin (Barnard, 2021). While outside the G-LiHT study area but in the same sub-region, Tikal reflects the same value (0.62) (Kohler et al., 2018, 294; Thompson et al., 2021b, 14).

Other regions sampled by the G-LiHT study have not undergone the same degree of quantification of Gini indices. In Chiapas, for example, Palenque's Gini coefficient has been reported as 0.44 based on structure area (Brown et al., 2012; Hutson, 2016; Strawinska-Zanko et al., 2018), slightly higher than the Río Candelaria-Río San Pedro tiles in the G-LiHT, again suggesting lower Gini coefficients outside of the densest urban areas in this part of the Western Lowlands. At El Infiernito, Chiapas, a fortified village near Piedras Negras, Guatemala, the Preclassic period West Group was characterized by a Gini coefficient of 0.29, which increased to 0.37 in the site's Terminal Classic period Upper Group (Schroder, 2019, 386), based on structure area, consistent with values from the Highland Ranges and Valleys sub-region in the G-LiHT data. Finally, Jessica Munson and Jonathan Scholnick's (2022) calculations of Gini coefficients at Altar de Sacrificios are not directly comparable to the G-LiHT findings due to the data sources originating from burials rather than house size, but the values range from 0.15 to 0.99, highlighting the importance of calculating Gini coefficients through

several different metrics to characterize differentiation.

Although the G-LiHT data do not include LiDAR in Belize, our results shown in Fig. 6, comparing Gini coefficients across the 6 metrics (structure footprint area and volume, patio group area and volume, and structure area and volume in patio groups) align closely with results shown in Table 4 of Amy Thompson and colleagues' (2021a) research in southern Belize. For example, Gini coefficients calculated based on structure area range from 0.14 to 0.45 in the G-LiHT and from 0.27 to 0.38 across the 8 sites in Belize (Uxbenká, Ix Kuku'il, Muklebal Tzul, Nimli Punit, Xnaheb, Lubaantun, Ek Xux, and Kaq'ru' Ha'). Meanwhile, the values calculated from structure volume range from 0.24 to 0.84 in the G-LiHT and from 0.33 to 0.62 at the sites in southern Belize. Structure area (0.19 to 0.60 in the G-LiHT, 0.31 to 0.55 in southern Belize) and structure volume in patio groups or plazuelas (0.24 to 0.82 in the G-LiHT, 0.29 to 0.75 in southern Belize) show similar trends. Comparable results are reported in Thompson and colleagues (2021b). Findings from Caracol (0.34 based on structure area and 0.6 based on structure volume) are also well in line with our findings across the G-LiHT dataset (Chase, 2017). Furthermore, we expect to test and improve the results of the current analysis by expanding the G-LiHT sampling in targeted areas with UAV LiDAR to explore more fully the surrounding archaeological and ecological context of tiles (Murtha et al., 2019; Schroder et al., 2021a, 2021b). Despite the limitations and complications of calculating Gini coefficients that we have outlined in this study, the consistency in results across Maya sub-regions and research projects is heartening and shows potential for the methodology. Again, the calculation of Gini coefficients is relatively straightforward, while the interpretation remains the true challenge.

The scope of the G-LiHT data enables a regional comparison of multiple variables that can be used as proxies for examining differentiation or wealth inequality. The advantages of big data approaches are clear: the same researchers can use the same information to systematically develop a comparative, region-wide dataset. However, a challenge of this big data approach lies in the volume of analytic datasets and visualizations created. For example, each metric (e.g. structure area, patio group volume, etc.) can be used to produce a distinct Lorenz curve for each tile in the dataset. Applied across the entire dataset, this would produce far too many visualizations to be meaningfully compared in a single paper. Yet, the strength of this approach is that these calculations and visualizations can be used as a baseline from which to further investigate how inequality and settlement patterns manifest at more localized spatial scales. Future studies might also investigate the potential of combining the results presented here with alternate measures of wealth, population distributions, and inequality. Calculating Gini coefficients offers insights into overall levels of inequality, while looking at the shape of wealth distributions can reveal more about how inequality was experienced across a community. For example, Strawinska-Zanko and colleagues (2018, 186) test for Pareto or powerlaw distributions as ways of understanding how wealth is distributed within Maya communities alongside Lorenz curves and Gini coefficients. Ideal Distribution Models (IDM) such as the Ideal Free Distribution (IFD) and others are additional models that are increasingly used by archaeologists and anthropologists to examine inequality in settlement and distribution patterns (Weitzel and Codding, 2022). Prufer and colleagues (2017) applied distribution models to settlement systems at Uxbenká, suggesting promise for further applications across the Maya area. Future studies integrating multiple measures of inequality applied across the regional analysis presented here will further clarify what the calculated Gini coefficients might mean in context.

While this study is a regional comparison of inequality, using measures of differentiation, we caution interpretations of comparisons of Gini indices across diverse spatial and time scales. Discretion must be exercised when comparing cultures with distinct architectural traditions if houses are to be used as an inequality metric (Basri and Lawrence, 2020, 690). The current study has benefited from a nearly continuous cross-section of the Maya landscape, aiding in regional comparisons

across the G-LiHT dataset, although additional integration with site-based approaches will be necessary to extrapolate findings outside of the G-LiHT flight paths. Temporality continues to be a challenging dimension when interpreting the G-LiHT data, which will require ongoing closer inspection of the LiDAR data, integration with site-based approaches, in-depth knowledge of local cultural histories and architectural form, and ground verification. With increasing access to large remotely sensed datasets and LiDAR, we can gather more complete and more accurate datasets of settlement. Basic statistics related to settlement, for example population estimates, feature density, and Gini indices, are simple enough to calculate, but interpretations of inequality will require multimodal evidence and collaboration to interpret how social differences manifest across the landscape.

#### CRediT authorship contribution statement

Whittaker Schroder: Conceptualization, Data curation, Formal analysis, Investigation, Methodology, Visualization, Writing - original draft, Writing - review & editing. Timothy Murtha: Data curation, Funding acquisition, Investigation, Project administration, Resources, Supervision, Validation, Writing - review & editing. Charles Golden: Funding acquisition, Writing - review & editing. Madeline Brown: Validation, Writing - original draft, Writing - review & editing. Robert Griffin: Funding acquisition, Writing - review & editing. Kelsey E. Herndon: Writing - review & editing. Shanti Morell-Hart: Funding acquisition, Writing - review & editing. Andrew K. Scherer: Funding acquisition, Writing - review & editing.

## **Declaration of Competing Interest**

The authors declare that they have no known competing financial interests or personal relationships that could have appeared to influence the work reported in this paper.

### Acknowledgments

Research funding was provided by the National Science Foundation (BCS#1849921) and the National Aeronautics and Space Administration (19-IDS19-0060). Dr. Hank Margolis (NASA Headquarters, Program Manager, NASA Terrestrial Ecology Program) collected LiDAR data with support from a NASA Carbon Cycle Science award to Ross Nelson (Program Announcement Number NNH10ZDA001N-CARBON). Field research in Mexico is supported by the Instituto Nacional de Antropología e Historia. This paper was presented in an earlier form in a conference session co-organized by Adrian Chase and Amy Thompson. We thank the anonymous reviewers for offering their insights to improve an earlier version of this manuscript.

#### Funding

Funding has been provided by the National Science Foundation, United States (BCS#1849921) and the National Aeronautics and Space Administration, United States (19-IDS19-0060).

# Appendix A. Supplementary material

Supplementary data to this article can be found online at https://doi.org/10.1016/j.jaa.2023.101552.

#### References

Abrams, E.M., 1994. How the Maya built their world: energetics and ancient architecture. University of Texas Press, Austin.

Amiel, Y., Cowell, F.A., 1999. Thinking about inequality: personal judgment and income distributions. Cambridge University Press, Cambridge.

Ashmore, W., 1981. Lowland Maya settlement patterns. School of American Research, Albuquerque.

- Ashmore, W., 1991. Site-planning principles and concepts of directionality among the ancient Maya. Lat. Am. Antiq. 2 (3), 199–226. https://doi.org/10.2307/972169.
- Ashmore, W., Willey, G.R., 1981. A historical introduction to the study of lowland Maya settlement patterns. In: Ashmore, W. (Ed.), Lowland Maya Settlement Patterns. University of New Mexico Press, Albuquerque, pp. 3–18.
- Barnard, E., 2021. Wealth inequality and market exchange: a household-based approach to the economy of Late Classic Uxul, Campeche. Archaeol. Papers Am. Anthropol. Assoc. 32 (1), 143–156. https://doi.org/10.1111/apaa.12149.
- Basri, P., Lawrence, D., 2020. Wealth inequality in the ancient Near East: a preliminary assessment using Gini coefficients and household size. Camb. Archaeol. J. 30 (4), 689–704. https://doi.org/10.1017/S0959774320000177.
- Beach, T., Luzzadder-Beach, S., Cook, D., Dunning, N., Kennett, D.J., Krause, S., Terry, R., Trein, D., Valdez, F., 2015. Ancient Maya impacts on the Earth's surface: an early Anthropocene analog? Quat. Sci. Rev. 124, 1–30. https://doi.org/10.1016/ i.guascirev.2015.05.028.
- Beck, J., Quinn, C.P., 2022. Balancing the scales: archaeological approaches to social inequality. World Archaeol. 54 (4), 572–583. https://doi.org/10.1080/ 00438243.2023.2169341.
- Blackmore, C., 2011a. Ritual among the masses: deconstructing identity and class in an ancient Maya neighborhood. Lat. Am. Antiq. 22 (2), 159–177. https://doi.org/10.7183/1045-6635.22.2.159.
- Blackmore, C., 2011b. How to queer the past without sex: queer theory, feminisms and the archaeology of identity. Archaeologies 7, 75–96. https://doi.org/10.1007/ s11759-011-9157-9.
- Bogaard, A., Fochesato, M., Bowles, S., 2019. The farming-inequality nexus: new insights from ancient Western Eurasia. Antiquity 93 (371), 1129–1143. https://doi.org/ 10.15184/aqy.2019.105.
- Boserup, E., 1965. The conditions of agricultural growth: the economics of agrarian change under population pressure. Allen and Unwin, London.
- Bourdieu, P., 1986. The forms of capital. In: Richardson, J. (Ed.), Handbook of theory and Research for the Sociology of Education. Greenwood, New York, pp. 241–258.
- Bowles, S., Carlin, W., 2017. Inequality as difference: a teaching note on the Gini coefficient. SFI Working Paper 2017-02-003, 1–8.
- Brown, C.T., Watson, A.A., Gravlin-Beman, A., Liebovitch, L.S., 2012. Poor Mayapan. In: Braswell, G.E. (Ed.), the Ancient Maya of Mexico: Reinterpreting the Past of the Northern Maya Lowlands. Equinox Publishing, Sheffield and Bristol, pp. 306–324.
- Canuto, M., Estrada-Belli, F., Garrison, T.G., Houston, S.D., Acuña, M.J., Kováč, M., Marken, D., Nondédéo, P., Auld-Thomas, L., Castanet, C., Chatelain, D., Chiriboga, C. R., Drápela, T., Lieskovský, T., Tokovinine, A., Velasquez, A., Fernández-Díaz, J.C., Shrestha, R., 2018. Ancient lowland Maya complexity as revealed by airborne laser scanning of northern Guatemala. Science 361 (6409), eaau0137. https://doi.org/10.1126/science.aau0137.
- Chakravarty, S.R., 1990. Ethical social index numbers. Springer-Verlag, New York.
  Chase, A.S.Z., 2017. Residential inequality among the ancient Maya: operationalizing household architectural volume at Caracol, Belize. Research Reports in Belizean Archaeology 14, 31–39.
- Chase, A.F., Chase, D.Z., 1996. A mighty Maya nation: how Caracol built an empire by cultivating its "middle class". Archaeology 49 (5), 66–72.
- Chase, A.F., Chase, D.Z., Fisher, C.T., Leisz, S.J., Weishampel, J.F., 2012. Geospatial revolution and remote sensing LiDAR in Mesoamerican archaeology. Proc. Natl. Acad. Sci. 109 (32), 12916–12921. https://doi.org/10.1073/pnas.1205198109.
- Chase, A.S.Z., Thompson, A.E., Walden, J.P., Feinman, G.M., forthcoming. Understanding and calculating household size, wealth, and inequality in the Maya Lowlands. Ancient Mesoamerica.
- Chen, J.J., Cortina, H., 2020. gglorenz: Plotting Lorenz curve with the blessing of "ggplot2." https://jjchern.github.io/gglorenz.
- Chi, M., Plaza, A., Benediktsson, J.A., Sun, Z., Shen, J., Zhu, Y., 2016. Big data for remote sensing: challenges and opportunities. Proc. IEEE 104 (11), 2207–2219. https://doi. org/10.1109/JPROC.2016.2598228.
- Cook, B., Corp, L., Nelson, R., Middleton, E., Morton, D., McCorkel, J., Masek, J., Ranson, K., Ly, V., Montesano, P., 2013. NASA Goddard's LIDAR, hyperspectral and thermal (G-LiHT) airborne imager. Remote Sens. (Basel) 5 (8), 4045–4066. https://doi.org/10.3390/rs5084045.
- Coulter, P.B., 1989. Measuring inequality: a methodological handbook. Routledge, New
- Deltas, G., 2003. The small sample bias of the Gini coefficient: results and implications for empirical research. Rev. Econ. Stat. 85 (1), 226–234. https://www.jstor.org/stable/3211637.
- Dixon, P.M., Weiner, J., Mitchell-Olds, T., Woodley, R., 1987. Boot-strapping the Gini coefficient of inequality. Ecology 68 (5), 1548–1551. https://doi.org/10.2307/ 1939238.
- Dorfman, R., 1979. A formula for the Gini coefficient. Rev. Econ. Stat. 61 (1), 146–149. https://doi.org/10.2307/1924845.
- Driver, W.D., Garber, J.F., 2004. The emergence of minor centers in the zones between seats of power. In: Garber, J.F. (Ed.), the ancient Maya of the Belize Valley: Half a Century of Archaeological Research. University Press of Florida, Gainesville, pp. 287–304.
- Estrada-Belli, F., Gilabert-Sansalvador, L., Canuto, M.A., Šprajc, I., Fernandez-Diaz, J.C., 2023. Architecture, wealth and status in Classic Maya urbanism revealed by airborne lidar mapping. J. Archaeol. Sci. 157, 105835 https://doi.org/10.1016/j. jas.2023.105835.
- Evans, D., 2016. Airborne laser scanning as a method for exploring long-term socioecological dynamics in Cambodia. J. Archaeol. Sci. 74, 164–175. https://doi.org/ 10.1016/j.jas.2016.05.009.

- Fick, S.E., Hijmans, R.J., 2017. WorldClim 2: new 1km spatial resolution climate surfaces for global land areas. Int. J. Climatol. 37 (12), 4302–4315. https://doi.org/10.1002/ ioc.5086
- Flannery, K., Marcus, J., 2012. The creation of inequality: how our prehistoric ancestors set the stage for monarchy, slavery, and empire. Harvard University Press, Cambridge.
- Foias, A.E., 2013. Ancient Maya political dynamics. University Press of Florida, Gainesville.
- Garrison, T.G., Houston, S.D., Scherer, A.K., del Cid, D., Garrido López, J.L., Czapiewska-Halliday, E., Román, E., 2016. A royal Maya country house: archaeology at Bejucal Guatemala. J. Field Archaeol. 41 (5), 532–549. https://doi.org/10.1080/ 00934690.2016.1219213.
- Garrison, T.G., Houston, S.D., Alcover Firpi, O., 2019. Recentering the rural: Lidar and articulated landscapes among the Maya. J. Anthropol. Archaeol. 53, 133–146. https://doi.org/10.1016/j.jaa.2018.11.005.
- Garrison, T.G., Thompson, A.E., Krause, S., Eshleman, S., Fernandez-Diaz, J.C., Baldwin, J.D., Cambranes, R., 2023. Assessing the lidar revolution in the Maya lowlands: a geographic approach to understanding feature classification accuracy. Prog. Phys. Geogr. 47 (2), 270–292. https://doi.org/10.1177/03091333221138050.
- Gastwirth, J.L., 1972. The estimation of the Lorenz curve and the Gini index. Rev. Econ. Stat. 54 (3), 306–316. https://doi.org/10.2307/1937992.
- Gini, C., 1912. Variabilità e mutabilità; contributo allo studio delle distribuzioni e delle relazioni statistiche. Tipogr. di P, Cuppini, Bologna.
- Giorgi, G.M., 1990. Gini coefficient. METRON International Journal of. Statistics 48 (1–4), 183–221.
- Glover, J.B., Rissolo, D., 2023. Coastal settlements and identities and the rise of the Itza. In: Stanton, T.W., Taube, K.A., Coltman, J.D., Marengo, N.I. (Eds.), When East Meets West: Chichen Itza, Tula, and the Postclassic Mesoamerican World. BAR International Series, Oxford, pp. 409–426.
- Golden, C., Murtha, T., Cook, B., Shaffer, D.S., Schroder, W., Hermitt, E.J., Alcover Firpi, O., Scherer, A.K., 2016. Reanalyzing environmental lidar data for archaeology: Mesoamerican applications and implications. J. Archaeol. Sci. Rep. 9, 293–308. https://doi.org/10.1016/j.jasrep.2016.07.029.
- Golden, C., Scherer, A., Schroder, W., Vella, C., Roche Recinos, A., 2020. Decentralizing the economies of the Maya west. In: Masson, M.A., Freidel, D.A., Demarest, A.A. (Eds.), The Real Business of Ancient Maya Economies: From Farmers' Fields to Rulers' Realms. University Press of Florida, Gainesville, pp. 403–417.
- Golden, C., Scherer, A.K., Schroder, W., Murtha, T., Morell-Hart, S., Fernandez Diaz, J.C., Jiménez Álvarez, S.D., Alcover Firpi, O., Agostini, M., Bazarsky, A., Clark, M., Kollias, G.V., Matsumoto, M., Roche Recinos, A., Schnell, J., Whitlock, B., 2021. Airborne Lidar Survey, Density-Based Clustering, and Ancient Maya Settlement in the Upper Usumacinta River Region of Mexico and Guatemala. Remote Sens. (Basel) 13 (20), 4109. https://doi.org/10.3390/rs13204109.
- Graeber, D., 2011. Debt: the first five thousand years. Melville House, New York. Harrison-Buck, E., Hendon, J.A., 2018. An introduction to relational personhood and other-than-human agency in archaeology. In: Harrison-Buck, E., Hendon, J.A. (Eds.), Relational Identities and Other-than-human Agency in Archaeology. University Press of Colorado, Boulder, pp. 3–28.
- Houston, S.D., Inomata, T., 2009. The Classic Maya. Cambridge University Press, Cambridge.
- Hutson, S.R., 2016. The ancient urban Maya: neighborhoods, inequality, and built form. University Press of Florida, Gainesville.
- Hutson, S.R., 2020. Inequality and social groups. In: Hutson, S.R., Ardren, T. (Eds.), The Maya World. Routledge, Oxon and New York, pp. 407–423.
- Hutson, S.R., Dunning, N.P., Cook, B., Ruhl, T., Barth, N.C., Conley, D., 2021. Rural settlement patterns, household cooperation, and regional subsistence interdependency in the Rio Bec area, Mexico: Contributions from G-LiHT. J. Anthropol. Res. 77 (4), 550–579. https://doi.org/10.1086/716750.
- Hutson, S., Chase, A.S.Z., Glover, J., Ringle, W., Stanton, T., 2023. Settlement scaling in the Northern Maya Lowlands: human-scale implications. Latin American Antiquity, 1–8. https://doi.org/ 10.1017/laq.2022.103.
- Hutson, S.R., Welch, J., 2021. Old urbanites as new urbanists? Mixing at an Ancient Maya city. J. Urban Hist. 47 (4), 812–831. https://doi.org/10.1177/ 0096144219879931.
- INEGI, 2000. Carta hidrología. https://www.inegi.org.mx/temas/hidrología.
- Inomata, T., 2006. Plazas, performers, and spectators. Curr. Anthropol. 47 (5), 805–842. https://doi.org/10.1086/506279.
- Inomata, T., Houston, S.D., 2018. Opening the royal Maya court. In: Inomata, T., Houston, S.D. (Eds.), Royal Courts of the Ancient Maya, Volume One: Theory, Comparison, and Synthesis. Routledge, New York, pp. 3–26.
- Inomata, T., Pinzón, F., Ranchos, J.L., Haraguchi, T., Nasu, H., Fernández-Diaz, J.C., Aoyama, K., Yonenobu, H., 2017. Archaeological Application of Airborne LiDAR with Object-Based Vegetation Classification and Visualization Techniques at the Lowland Maya Site of Ceibal. Guatemala. Remote Sensing 9 (6), 563. https://doi. org/10.3390/rs9060563.
- Jackson, S.E., 2013. Politics of the Maya court: hierarchy and change in the Late Classic period. University of Oklahoma Press, Norman.
- Kintigh, K.W., Altschul, J.H., Beaudry, M.C., Drennan, R.D., Kinzig, A.P., Kohler, T.A., Limp, W.F., Maschner, H.D.G., Michener, W.K., Pauketat, T.R., Peregrine, P., Sabloff, J.A., Wilkinson, T.J., Wright, H.T., Zeder, M.A., 2014. Grand challenges for archaeology. Am. Antiq. 79 (1), 5–24. https://doi.org/10.7183/0002-7316.79.1.5.
- Kohler, T.A., 1992. Field houses, villages, and the tragedy of the commons in the early Northern Anasazi Southwest. Am. Antiq. 57 (4), 617–635. https://doi.org/10.2307/
- Kohler, T.A., Smith, M.E., Bogaard, A., Peterson, C.E., Betzenhauser, A., Feinman, G.M., Oka, R.C., Pailes, M., Prentiss, A.M., Stone, E.C., Dennehy, T.J., Ellyson, L.J., 2018.

- Deep inequality: summary and conclusions. In: Kohler, T.A., Smith, M.E. (Eds.), Ten Thousand Years of Inequality: the Archaeology of Wealth Differences. University of Arizona Press, Tucson, pp. 289–317.
- Kohler, T.A., Smith, M.E., 2018. Ten thousand years of inequality: the archaeology of wealth differences. University of Arizona Press, Tucson.
- Kohler, T.A., Smith, M.E., Bogaard, A., Feinman, G.M., Peterson, C.E., Betzenhauser, A., Pailes, M., Stone, E.C., Prentiss, A.M., Dennehy, T.J., Ellyson, L.J., Nicholas, L.M., Faulseit, R.K., Styring, A., Whitlam, J., Fochesato, M., Foor, T.A., Bowles, S., 2017. Greater post-Neolithic wealth disparities in Eurasia than in North America and Mesoamerica. Nature 551, 619–622. https://doi.org/10.1038/nature24646.
- Kurnick, S., 2015. The origins of extreme economic inequality: an archaeologist's take on a contemporary controversy. Archaeologies 11, 400–416. https://doi.org/10.1007/ s11759-015-9282-v.
- Lacquement, C.H., 2010. Recalculating mound volume at Moundville. Southeast. Archaeol. 29 (2), 341–354. https://doi.org/10.1179/sea.2010.29.2.009.
- Lamoureux-St-Hilaire, M., 2022. The tapir in the room: ancient Maya storage architecture. J. Anthropol. Archaeol. 68, 101467 https://doi.org/10.1016/j. jaa.2022.101467.
- LeCount, L.J., Walker, C.P., Blitz, J.H., Nelson, T.C., 2019. Land tenure systems at the ancient Maya site of Actuncan. Belize. Latin American Antiquity 30 (2), 245–265. https://doi.org/10.1017/laq.2019.16.
- Liendo Stuardo, R., López Bravo, R., 2006. Organización política y funciones sociales vistas a través de los patios para el juego de pelota del señorío de Palenque. In: Laporte, J.P., Arroyo, B., Mejía, H. (Eds.), XIX Simposio De Investigaciones Arqueológicas En Guatemala, 2005. Museo Nacional de Arqueología y Etnología, Guatemala City, pp. 431–440.
- Liendo Stuardo, R., López Mejía, J., Campiani, A., 2014. The social construction of public spaces at Palenque and Chinikihá, Mexico. In: Tsukamoto, K., Inomata, T. (Eds.), Mesoamerican Plazas: Arenas of Community and Power. University of Arizona Press, Tucson, pp. 108–120.
- Liendo Stuardo, R., 2002. The organization of agricultural production at a Maya center: settlement patterns in the Palenque region, Chiapas, México, Serie Arqueología de México. Instituto Nacional de Antropología e Historia and University of Pittsburgh, Mexico City and Pittsburgh.
- Lorenz, M.O., 1905. Methods of measuring the concentration of wealth. Publ. Am. Stat. Assoc. 9 (70), 209–219. https://doi.org/10.2307/2276207.
- Magnani, M., Schroder, W., 2015. New approaches to modeling the volume of earthen archaeological features: a case study from the Hopewell culture mounds. J. Archaeol. Sci. 64, 12–21. https://doi.org/10.1016/j.jas.2015.09.001.
- Magnoni, A., Hutson, S.R., Dahlin, B., 2012. Living in the city: settlement patterns and the urban experience at Classic period Chunchucmil, Yucatan. Mexico. Ancient Mesoamerica 23 (2), 313–343. https://doi.org/10.1017/S0956536112000223.
- McAnany, P.A., 2013. Living with the ancestors: kinship and kingship in ancient Maya society, Revised edition. Cambridge University Press, New York.
- McGuire, R.H., 1983. Breaking down cultural complexity: inequality and heterogeneity. Adv. Archeol. Method Theory 6, 91–142. https://doi.org/10.1016/B978-0-12-003106-150008-0
- McGuire, R.H., 2022. Reflections on archaeology and inequality. A foreword. World Archaeology 54 (4), 491–492. https://doi.org/10.1080/00438243.2022.2233798.
- McGuire, R., Netting, R.M., 1982. Leveling peasants? The maintenance of equality in a Swiss Alpine community. Am. Ethnol. 9 (2), 269–290. https://www.jstor.org/stable/644676
- Midlarsky, M.I., 1999. The evolution of inequality: war, state survival, and democracy in comparative perspective. Stanford University Press, Stanford.
- Miller, M., Brittenham, C., 2013. The spectacle of the late Maya court: reflections on the murals of Bonampak. University of Texas Press, Austin.
- Munson, J., Scholnick, J., 2022. Wealth and Well-being in an Ancient Maya Community. J. Archaeol. Method Theory 29, 1–30. https://doi.org/10.1007/s10816-021-09508-8.
- Murtha, T.M., Broadbent, E.N., Golden, C., Scherer, A.K., Schroder, W., Wilkinson, B., Almeyda Zambrano, A., 2019. Drone-mounted Lidar survey of Maya settlement and landscape. Lat. Am. Antiq. 30 (3), 630–636. https://doi.org/10.1017/laq.2019.51.
- Nelson, Z., 2005. Settlement and population at Piedras Negras. Pennsylvania State University. Unpublished PhD dissertation).
- Netting, R.M., 1982. Some home truths about household size and wealth. Am. Behav. Sci. 25 (6), 641–662. https://doi.org/10.1177/000276482025006004.
- Paynter, R., 1989. The archaeology of equality and inequality. Ann. Rev. Anthropol. 18, 369–399. https://doi.org/10.1146/annurev.an.18.100189.002101.
- Peterson, C.E., Drennan, R.D., 2018. Letting the Gini out of the bottle: measuring inequality archaeologically. In: Kohler, T.A., Smith, M.E. (Eds.), Ten Thousand Years of Inequality: the Archaeology of Wealth Differences. University of Arizona Press, Tucson, pp. 39–66.
- Piketty, T., 2014. Capital in the twenty-first century. Harvard University Press, Cambridge.
- Piketty, T., 2020. Capital and ideology. The Belknap Press of Harvard University Press, Cambridge.
- Prufer, K.M., Thompson, A.E., Meredith, C.R., Culleton, B.J., Jordan, J.M., Ebert, C.E., Winterhalder, B., Kennett, D.J., 2017. The Classic period Maya transition from an ideal free to an ideal despotic settlement system at the polity of Uxbenká. J. Anthropol. Archaeol. 45, 53–68. https://doi.org/10.1016/j.jaa.2016.11.003.
- R Core Team, 2021. R: a language and environment for statistical computing. https://www.r-project.org.
- Ready, E., Power, E.A., 2018. Why wage earners hunt: food sharing, social structure, and influence in an Arctic mixed economy. Curr. Anthropol. 59 (1), 74–97. https://doi. org/10.1086/696018.

- Robin, C., 2003. New directions in Classic Maya household archaeology. J. Archaeol. Res. 11 (4), 307–356. https://doi.org/10.1023/A:1026327105877.
- Rogers, D.S., Deshpande, O., Feldman, M.W., 2011. The spread of inequality. PLoS One 6 (9), e24683.
- Rosenswig, R.M., López-Torrijos, R., Antonelli, C.E., Mendelsohn, R.R., 2013. Lidar mapping and surface survey of the Izapa state on the tropical piedmont of Chiapas. Mexico. Journal of Archaeological Science 40 (3), 1493–1507. https://doi.org/ 10.1016/j.jas.2012.10.034.
- Schroder, W., 2019. Community resilience through crisis at El Infiernito, Chiapas, a fortified refuge in the Upper Usumacinta valley. University of Pennsylvania. Unpublished PhD dissertation.
- Schroder, W., Murtha, T., Golden, C., Anaya Hernández, A., Scherer, A., Morell-Hart, S., Almeyda Zambrano, A., Broadbent, E.N., Brown, M., 2020. The Lowland Maya settlement landscape: environmental LiDAR and ecology. J. Archaeol. Sci. Rep. 33, 102543 https://doi.org/10.1016/j.jasrep.2020.102543.
- Schroder, W., Murtha, T., Broadbent, E.N., Almeyda Zambrano, A.M., 2021a. A confluence of communities: households and land use at the junction of the Upper Usumacinta and Lacantún Rivers. Chiapas, Mexico 53 (4), 688–715. https://doi.org/ 10.1080/00438243.2021.1930135.
- Schroder, W., Murtha, T., Golden, C., Scherer, A.K., Broadbent, E.N., Almeyda Zambrano, A.M., Herndon, K., Griffin, R., 2021b. UAV LiDAR survey for archaeological documentation in Chiapas Mexico. Remote Sens. 13 (23), 4731. https://doi.org/10.3390/rs13234731.
- Schulting, R.J., 1995. Mortuary variability and status differentiation on the Columbia-Fraser Plateau. Archaeology Press, Burnaby.
- Sen, A.K., 1973. On economic inequality. Oxford University Press, Delhi.
- Signorell, A., 2022. DescTools: tools for descriptive statistics. https://andrisignorell.github.io/DescTools/, https://github.com/AndriSignorell/DescTools.
- Smith, M.E., 1987. Household possessions and wealth in agrarian states: implications for archaeology. J. Anthropol. Archaeol. 6 (4), 297–335. https://doi.org/10.1016/ 0278-4165(87)90004-3.
- Smith, M.L., 2018. Urbanism and the Middle Class: co-emergent phenomena in the World's first cities. J. Anthropol. Res. 74 (3), 299–326. https://doi.org/10.1086/ 607656
- Smith, E.A., Borgerhoff Mulder, M., Bowles, S., Gurven, M., Hertz, T., Shenk, M.K., 2010. Production systems, inheritance, and inequality in premodern societies: conclusions. Curr. Anthropol. 51 (1), 85–94. https://doi.org/10.1086/649029.
- Smith, M., Dennehy, T., Kamp-Whittaker, A., Colon, E., Harkness, R., 2014. Quantitative Measures of Wealth Inequality in Ancient Central Mexican Communities. Adv. Archaeol. Pract. 2 (4), 311–323. https://doi.org/10.7183/2326-3768.2.4.XX.
- Smith, M.E., Kohler, T.A., Feinman, G.M., 2018. Studying inequality's deep past. In: Kohler, T.A., Smith, M.E., (Eds.), Ten Thousand Years of Inequality: the Archaeology of Wealth Differences. University of Arizona Press, Tucson, pp. 3–38.
- Smith, M.E., Ortman, S.G., Lobo, J., Ebert, C.E., Thompson, A.E., Prufer, K.M., Liendo Stuardo, R., Rosenswig, R.M., 2021. The low-density urban systems of the Classic period Maya and Izapa: insights from settlement scaling theory. Lat. Am. Antiq. 32 (1), 120–137. https://doi.org/10.1017/laq.2020.80.
- Stiglitz, J.E., 2015. The Great Divide: unequal societies and what we can do about them. New York, W.W, Norton and Company.
- Strawinska-Zanko, U., Liebovitch, L.S., Watson, A., Brown, C.T., 2018. Capital in the First Century: the evolution of inequality in Ancient Maya society. In: Strawinska-Zanko, U., Liebovitch, L.S. (Eds.), Mathematical Modeling of Social Relationships: What Mathematics Can Tell Us About People. Springer, Cham, pp. 161–192.
- Taschek, J.T., Ball, J.W., 2003. Nohoch Ek revisited: the minor center as manor. Lat. Am. Antiq. 14 (4), 371–388. https://doi.org/10.2307/3557574.
- Thompson, A.E., Prufer, K.M., 2021. Household inequality, community formation, and land tenure in Classic period lowland Maya society. J. Archaeol. Method Theory 28, 1276–1313. https://doi.org/10.1007/s10816-020-09505-3.
- Thompson, A.E., Feinman, G.M., Lemly, M., Prufer, K.M., 2021a. Inequality, networks, and the financing of Classic Maya political power. J. Archaeol. Sci. 133, 105441 https://doi.org/10.1016/j.jas.2021.105441.
- Thompson, A.E., Feinman, G.M., Prufer, K.M., 2021b. Assessing Classic Maya multiscalar household inequality in southern Belize. PLoS One 16 (3), e0248169.
- Trapeznikova, I., 2019. Measuring income inequality: summary measures of inequality differ from one another and give different pictures of the evolution of economic inequality over time. IZA World of Labor 462, 1–12. https://doi.org/10.15185/izawol.462.
- VanValkenburgh, P., Dufton, J.A., 2020. Big archaeology: horizons and blindspots 45, S1–S7. https://doi.org/10.1080/00934690.2020.1714307.
- Weitzel, E.M., Codding, B.F., 2022. The Ideal Distribution Model and archaeological settlement patterning. Environ. Archaeol. 27 (4), 349–356. https://doi.org/ 10.1080/14614103.2020.1803015.
- Wickham, H., 2016. ggplot2: elegant graphics for data analysis. Springer, New York.
  Wilk, R.R., 1983. Little house in the jungle: the causes of variation in house size among modern Kekchi Maya. J. Anthropol. Archaeol. 2 (2), 99–116. https://doi.org/10.1016/0278-4165(83)90009-0.
- Wilkerson, I., 2020. Caste: the origins of our discontents. Random House, New York.
  Windler, A., Thiele, R., Müller, J., 2013. Increasing inequality in Chalcolithic southeast
  Europe: the case of Durankulak. J. Archaeol. Sci. 40 (1), 204–210. https://doi.org/10.1016/j.jas.2012.08.017.

- Witschey, W.R.T., Brown, C., 2010. The electronic atlas of Maya sites. http://mayagis.
- smv.org.

  Xu, K., 2003. How has the literature on Gini's index evolved in the past 80 years?

  Dalhousie University, Economics Working Paper, pp. 1–41.
- Yu, S.-Y., 2019. Inferring inequality in prehistoric societies from grave sizes: a methodological framework. Archaeol. Anthropol. Sci. 11, 4947–4958. https://doi. org/10.1007/s12520-019-00845-0.